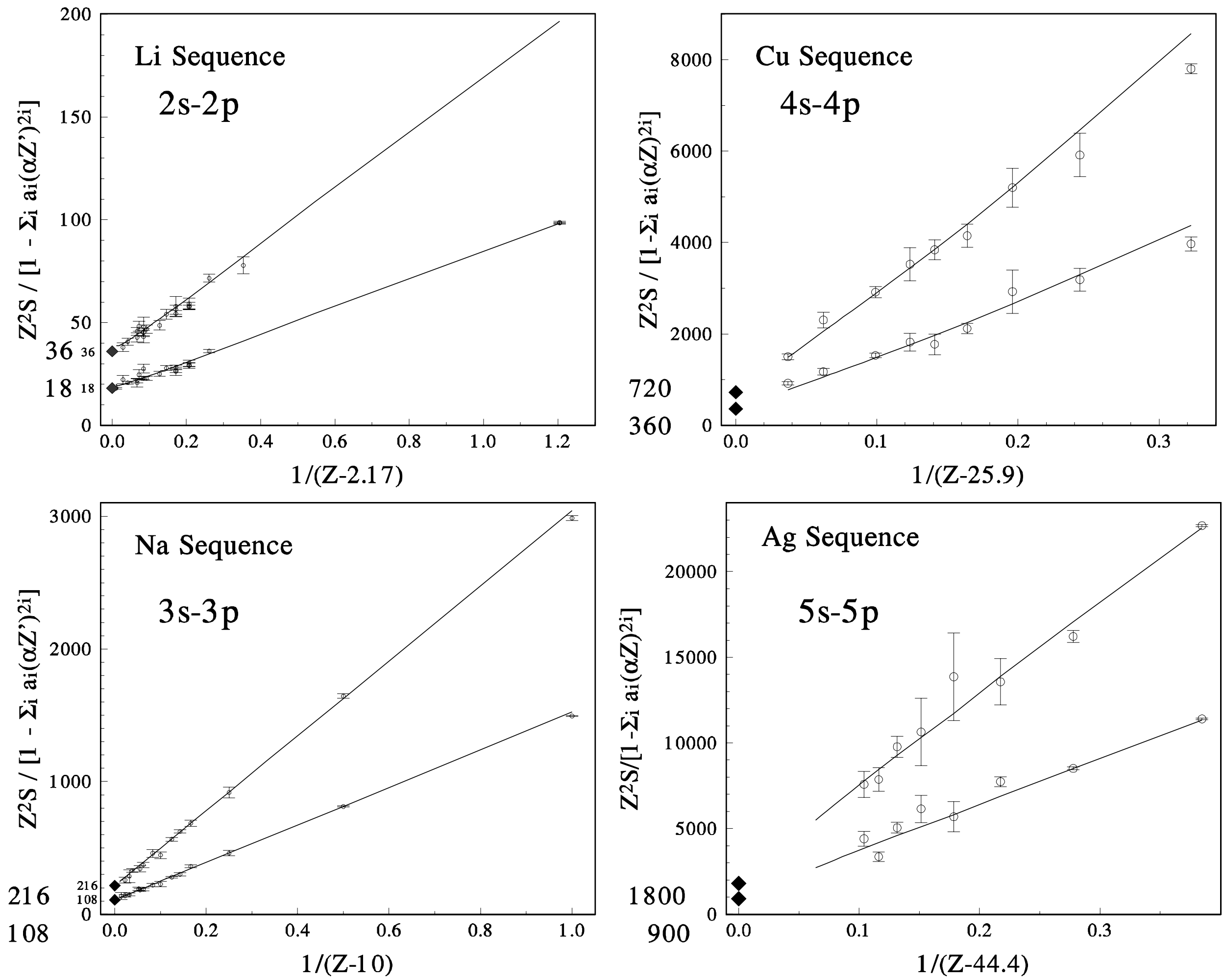
Li Sequence
2s-2p
Z²S / [1 - Σi ai(αZ')²ⁱ]
1/(Z-2.17)
36
18
Cu Sequence
4s-4p
Z²S / [1-Σi ai(αZ)²ⁱ]
1/(Z-25.9)
720
360
Na Sequence
3s-3p
Z²S / [1 - Σi ai(αZ')²ⁱ]
1/(Z-10)
216
108
Ag Sequence
5s-5p
Z²S/[1-Σi ai(αZ)²ⁱ]
1/(Z-44.4)
1800
900

$$Z^2 S = S_H \longrightarrow S_H + \frac{b}{Z-C}$$

H-like ... Alkalilike

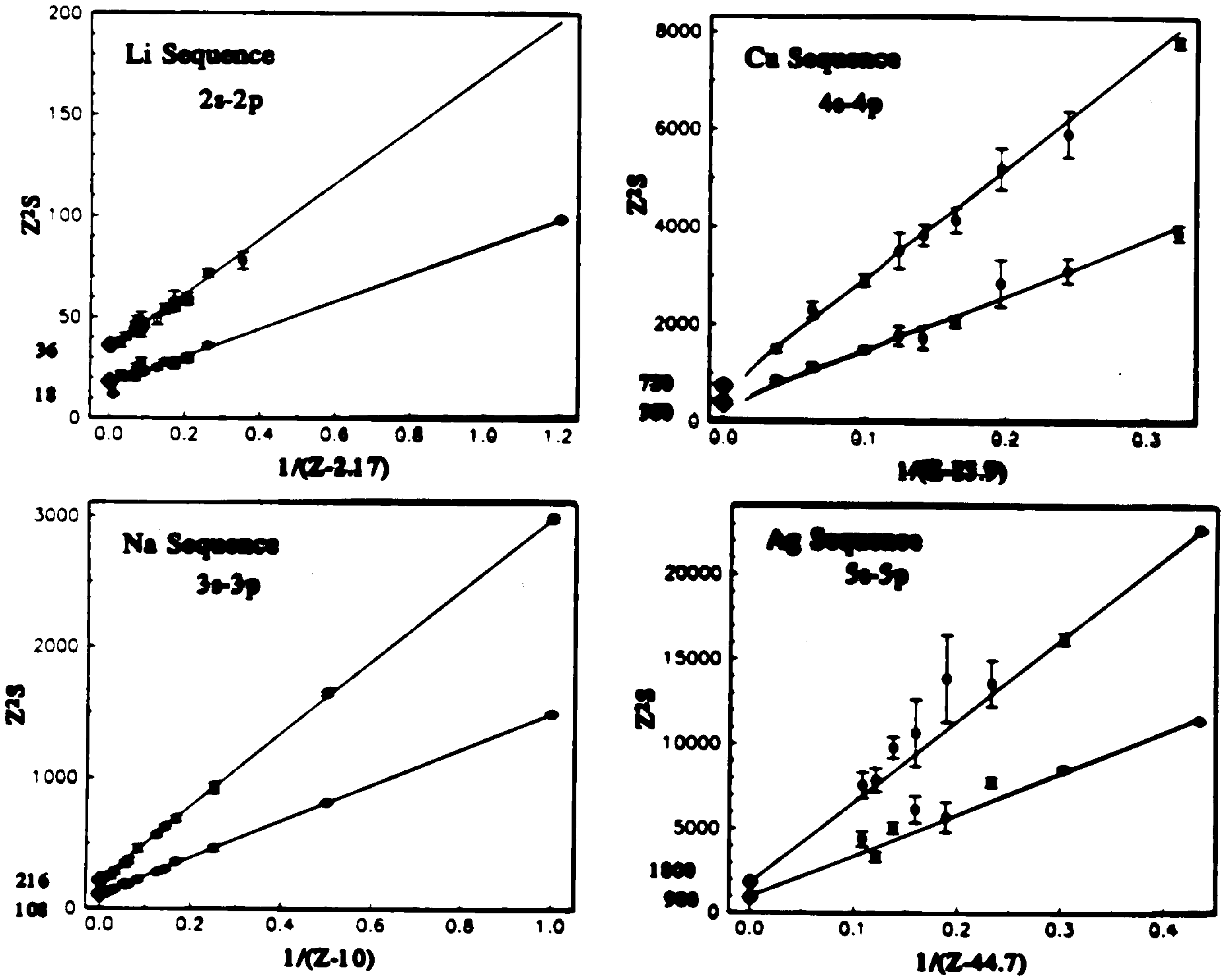

◆ $$S_H(ns-np) = \frac{3}{4} n^2 (n^2-1)(2J+1)$$

$$S_{ik} = \left[\frac{\lambda(\text{Å})}{1265.38}\right]^3 \frac{g_i B_{ik}}{\tau_i(ns)}$$

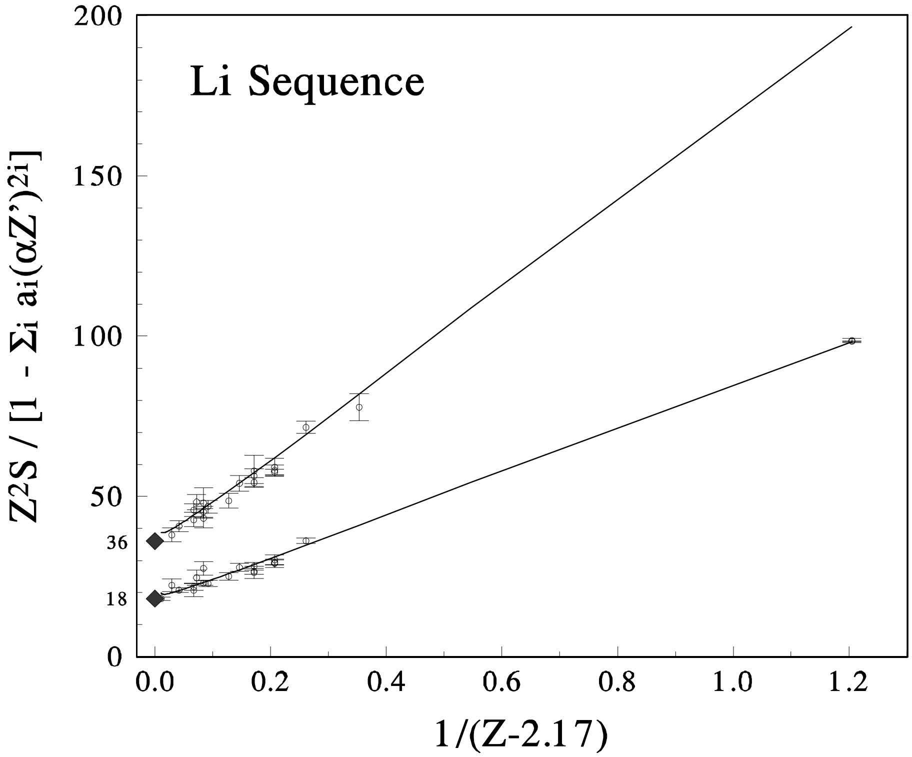

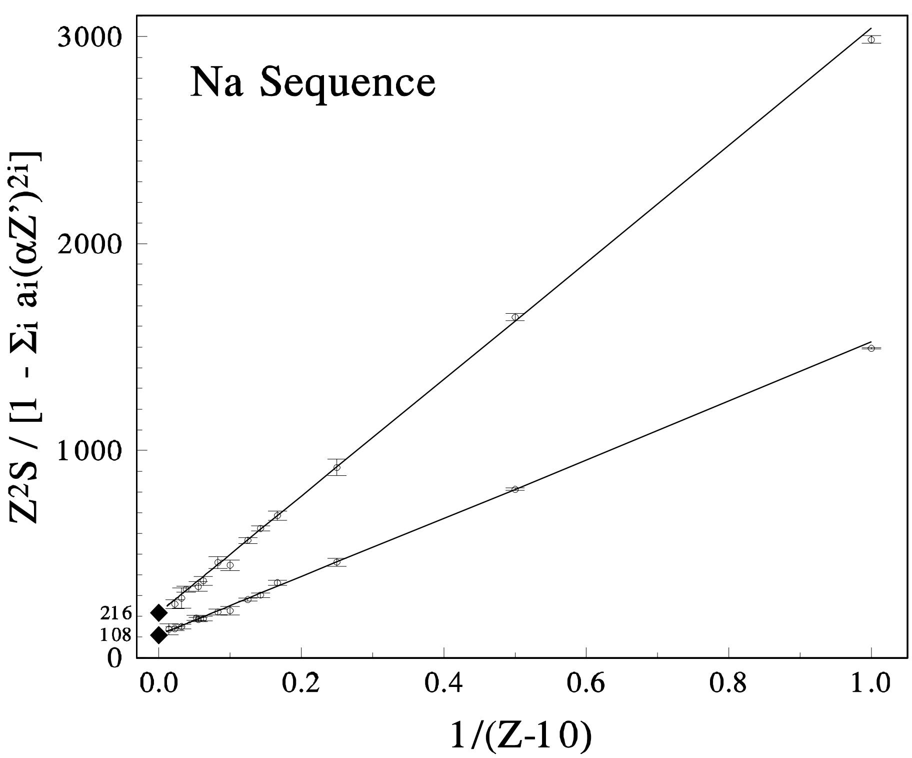

--- Johnson, Liu & Sapirstein, Atom.Data Nucl.Data Tables 64, 279-300 (1996).

Relativistic Hydrogenlike Line Strengths

$$Z^2 S_H^R(Z) = Z^2 S_H \left[1 - \sum_{i=1}^{\infty} a_i (\alpha Z)^{2i} \right]$$

TABLE I. Constants for relativistic hydrogelike line strengths.

Transition	$S_H(1)$	a_1	a_2	a_3	a_4	a_5
$2s_{1/2} - 2p_{1/2}$	18	5/6	-1/48	1/96	7/768	11/1536
$2s_{1/2} - 2p_{3/2}$	36	1/3	0.110187	0.059476	0.037032	0.024925
$3s_{1/2} - 3p_{1/2}$	108	7/12	5/144	7/288	37/2304	53/4608
$3s_{1/2} - 3p_{3/2}$	216	19/72	0.139267	0.082219	0.050840	0.033291
$4s_{1/2} - 4p_{1/2}$	360	9/20	3/64	17/640	87/5120	123/10240
$4s_{1/2} - 4p_{3/2}$	720	103/480	0.147237	0.093466	0.058853	0.038459
$5s_{1/2} - 5p_{1/2}$	900	11/30	29/600	31/1200	157/9600	221/19200
$5s_{1/2} - 5p_{3/2}$	1800	9/50	0.150012	0.100133	0.064068	0.041970

New plotting parameter

$$\frac{Z^2 S}{1 - \sum_i a_i [\alpha (Z-C)]^{2i}} \cong Z^2 S_H \left[A' + \frac{B'}{(Z-C)} \right]$$

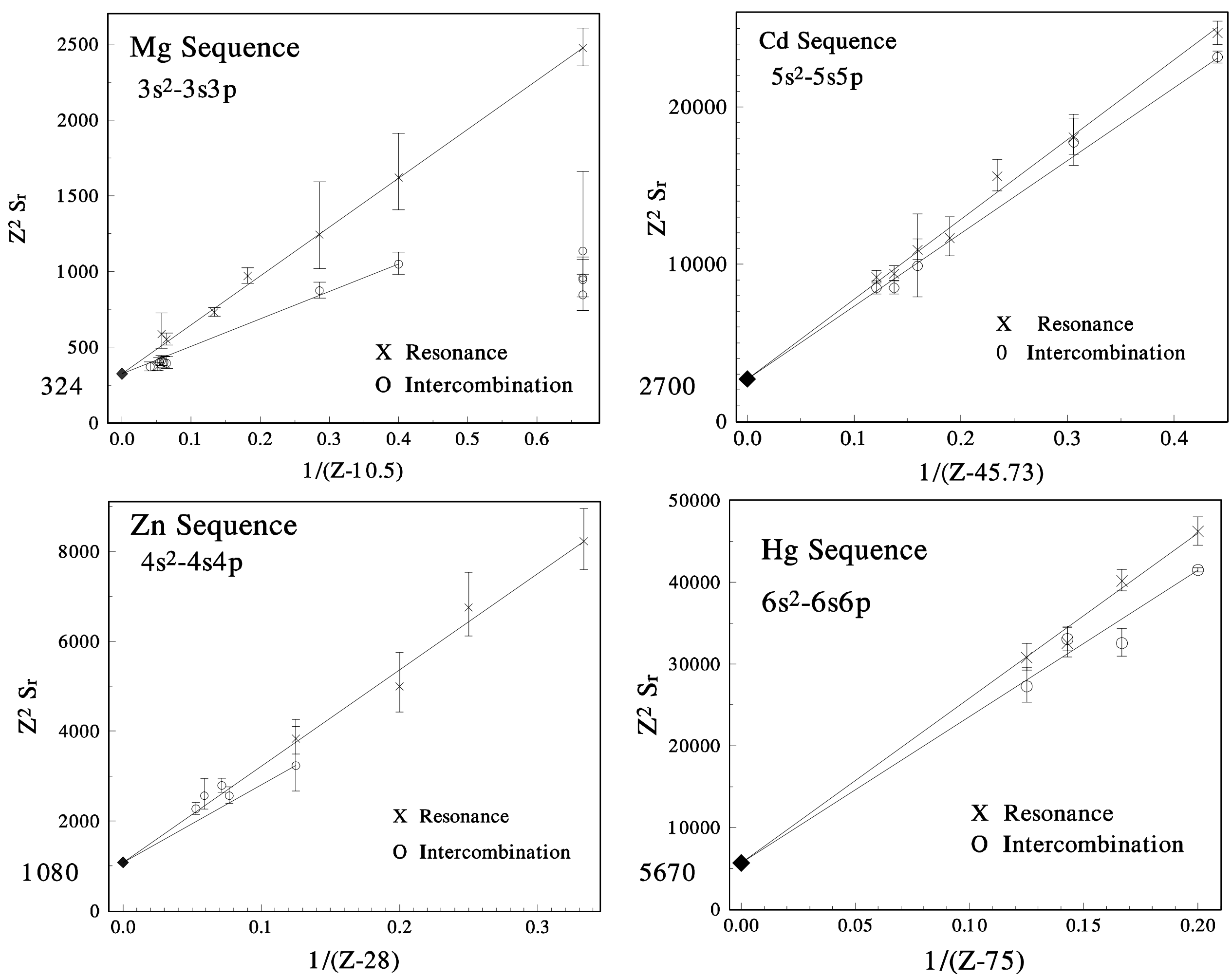

Mg Sequence
3s2-3s3p
X Resonance
O Intercombination
324
Z^2 Sr
1/(Z-10.5)
Cd Sequence
5s2-5s5p
X Resonance
0 Intercombination
2700
Z^2 Sr
1/(Z-45.73)
Zn Sequence
4s2-4s4p
X Resonance
O Intercombination
1080
Z^2 Sr
1/(Z-28)
Hg Sequence
6s2-6s6p
X Resonance
O Intercombination
5670
Z^2 Sr
1/(Z-75)

$$S_r(\text{Res}) = \frac{S(\text{Res})}{\cos^2\theta} \quad ; \quad S_r(\text{Int}) = \frac{S(\text{Int})}{\sin^2\theta}$$

θ determined from energy level data

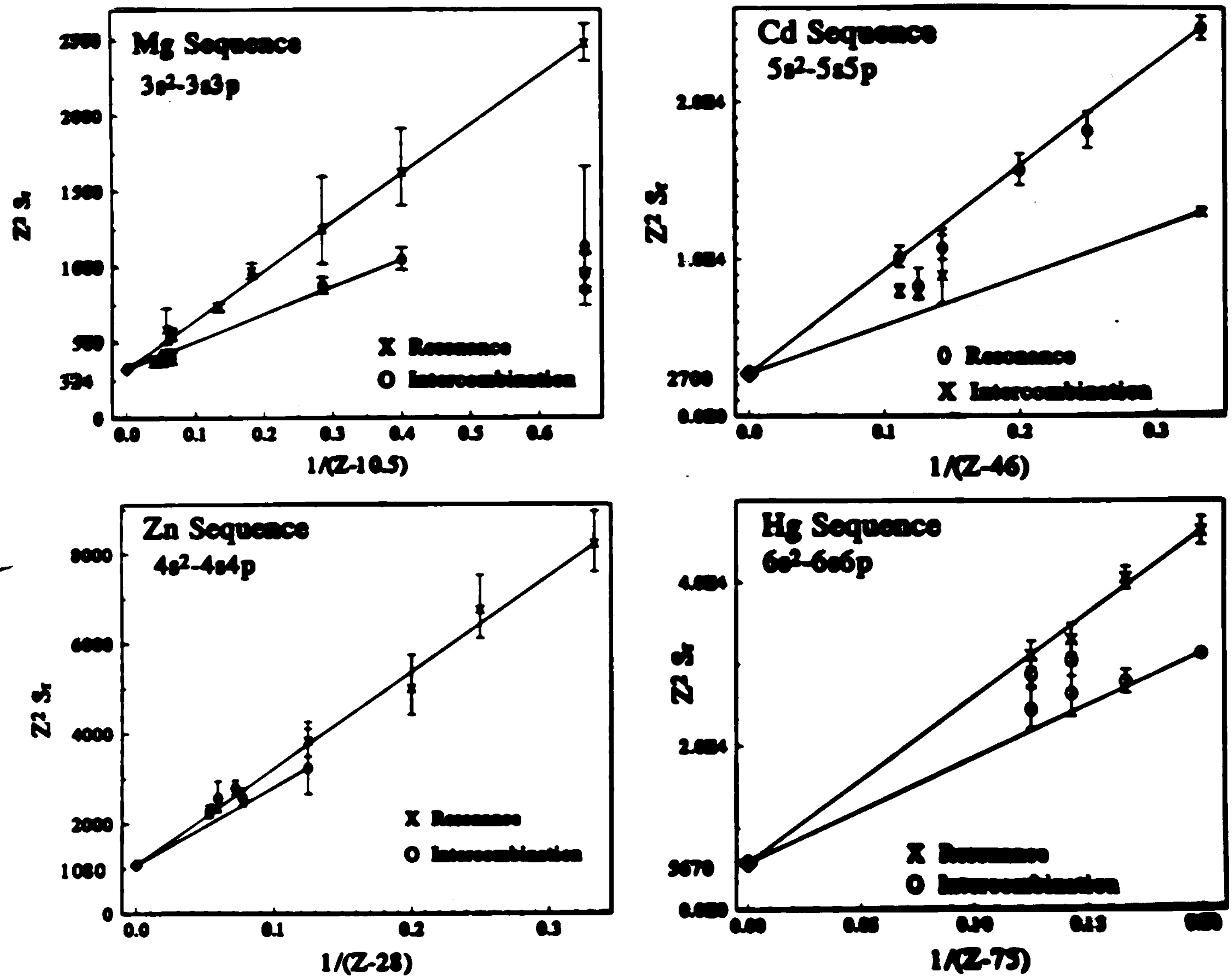

$$S_H = \frac{9}{2} n^2 (n^2 - 1)$$

Singlet-Triplet Mixing Angles

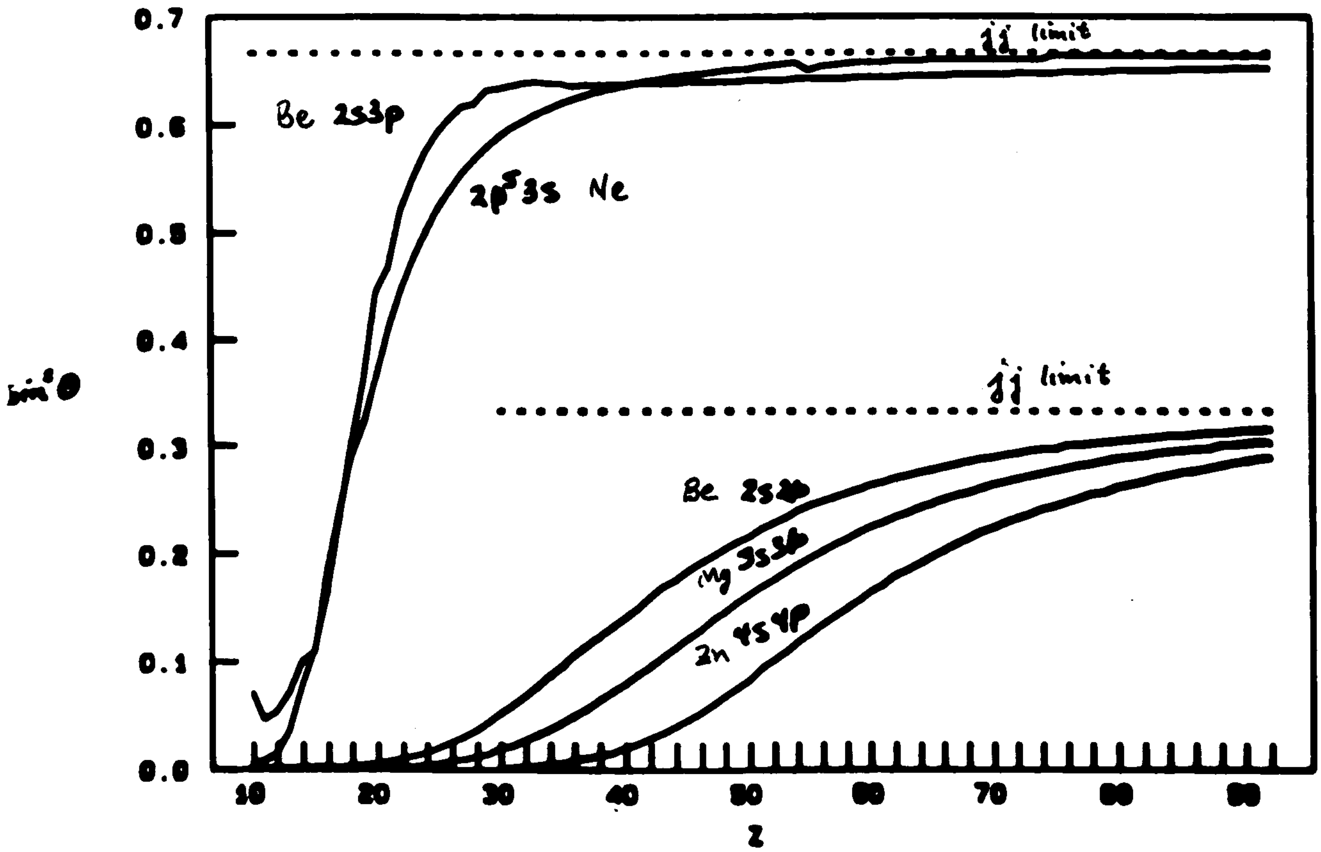

$$\cot(2\theta) = 1/\sqrt{8} + A(Z-C)^p$$

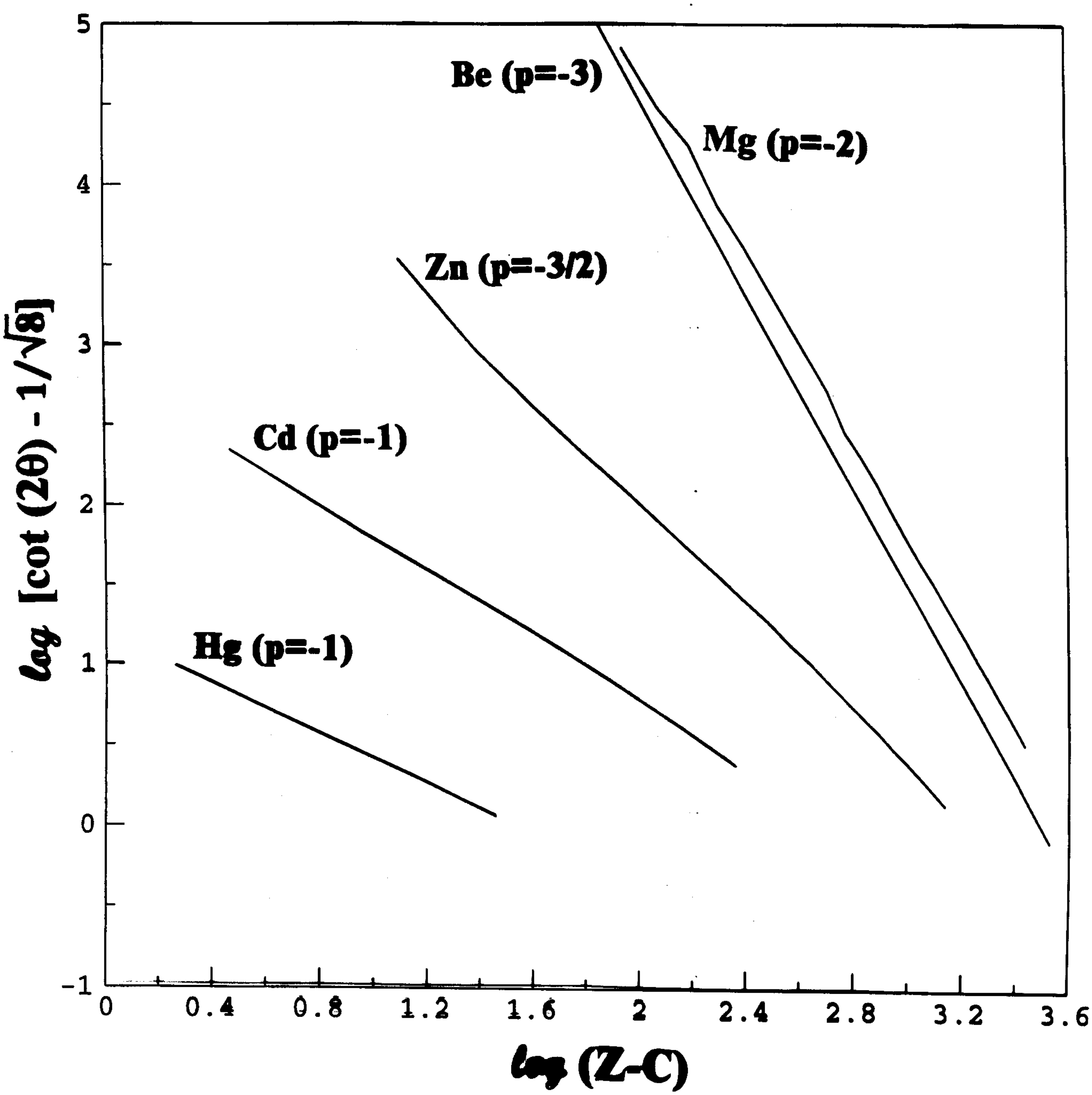

ns np

Hugh Wolfe PR 41, 443 (1932)

G.W. King & J.H. Van Vleck PR 56 464 (1939)

	$^3P_0$	$^3P_1$	$^3P_2$	$^1P_1$
$^3P_0$	$E_0-G_1-\mu_1$	0	0	0
$^3P_1$	0	$E_0-G_1-\mu_1/2$	0	$\mu_2/\sqrt{2}$
$^3P_2$	0	0	$E_0-G_1+\mu_1/2$	0
$^1P_1$	0	$\mu_2/\sqrt{2}$	0	E_0+G_1

This is diagonal in the representation

$$|^3P_0'\rangle = |^3P_0\rangle$$
$$|^3P_1'\rangle = \cos\theta_1\,|^3P_1\rangle - \sin\theta_1\,|^1P_1\rangle$$
$$|^3P_2'\rangle = |^3P_2\rangle$$
$$|^1P_1'\rangle = \sin\theta_1\,|^3P_1\rangle + \cos\theta_1\,|^1P_1\rangle$$

with energies

$$|^3P_0\rangle = E_0 - G_1 - \mu_1$$
$$|^3P_1'\rangle = E_0 - \mu_1/4 - \Delta$$
$$|^3P_2\rangle = E_0 - G_1 + \mu_1/2$$
$$|^1P_1'\rangle = E_0 - \mu_1/4 + \Delta$$
$$\Delta \equiv \sqrt{(G+\mu_1/4)^2 + \mu_2^2/2}$$

The determine the mixing angle

$$\cot 2\theta = \frac{4G_1 + \mu_1}{\sqrt{8}\,\mu_2}$$

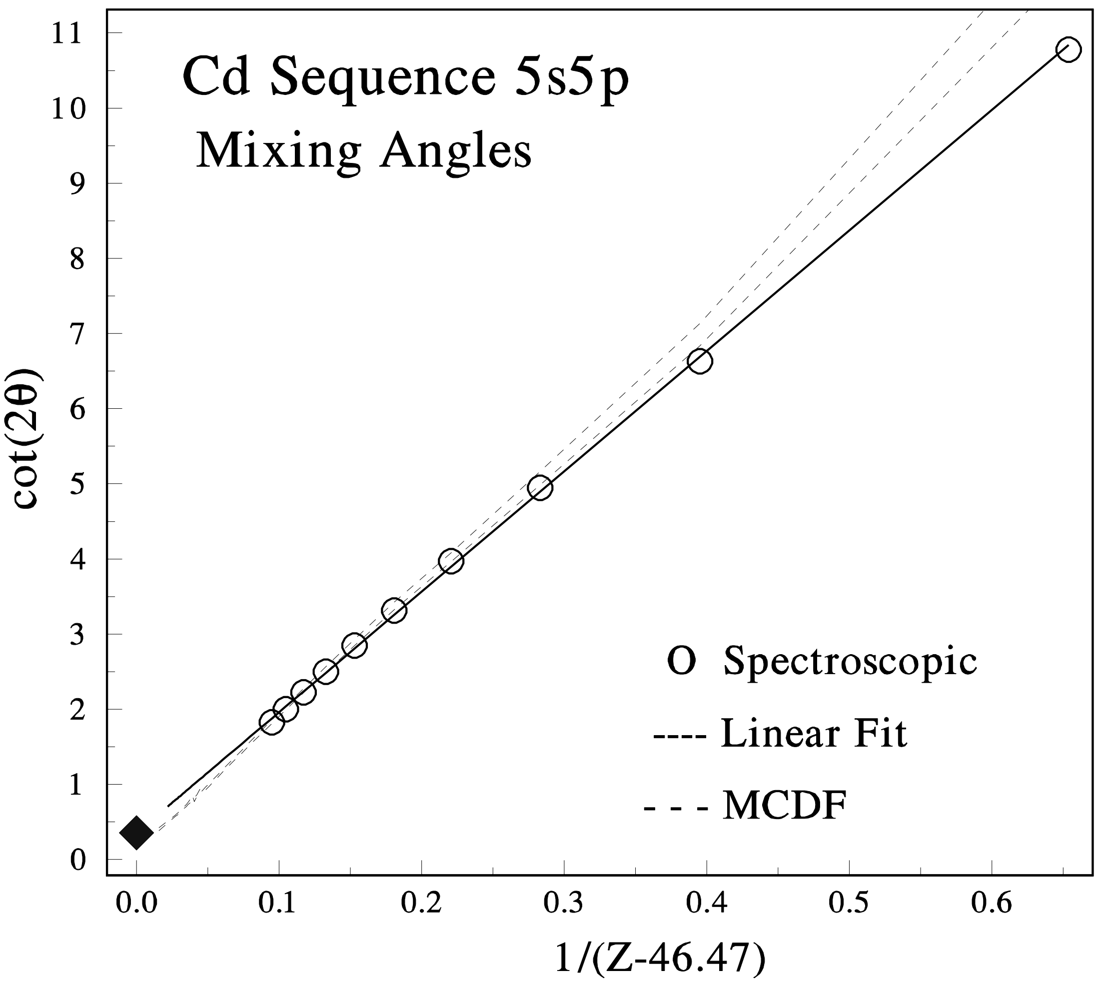

Cd Sequence 5s5p
Mixing Angles
O Spectroscopic
---- Linear Fit
- - - MCDF
cot(2θ)
1/(Z-46.47)
0
1
2
3
4
5
6
7
8
9
10
11
0.0
0.1
0.2
0.3
0.4
0.5
0.6

$5s^2\ ^1S_0 - 5s5p\ ^{1,3}P_1$ energy intervals

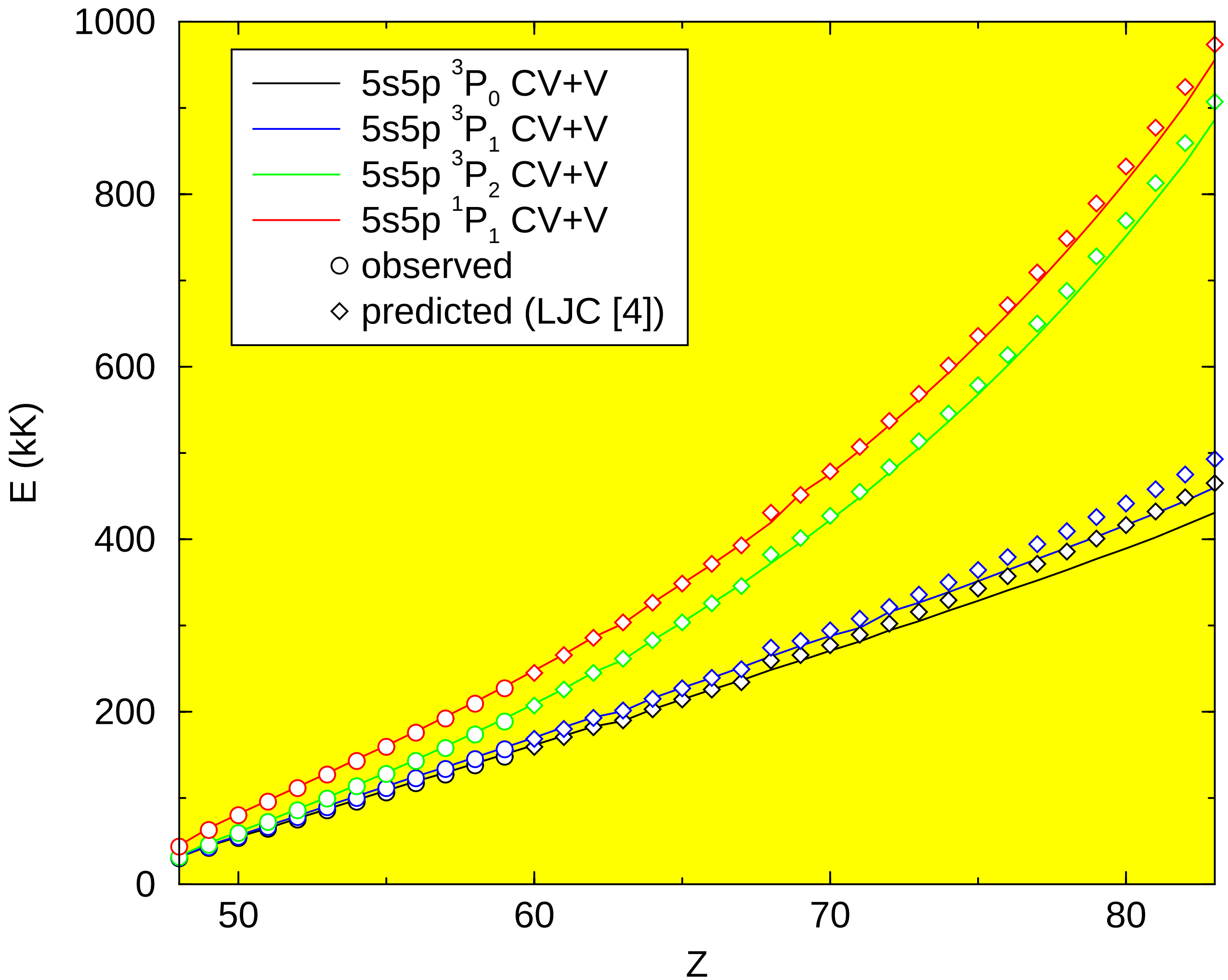

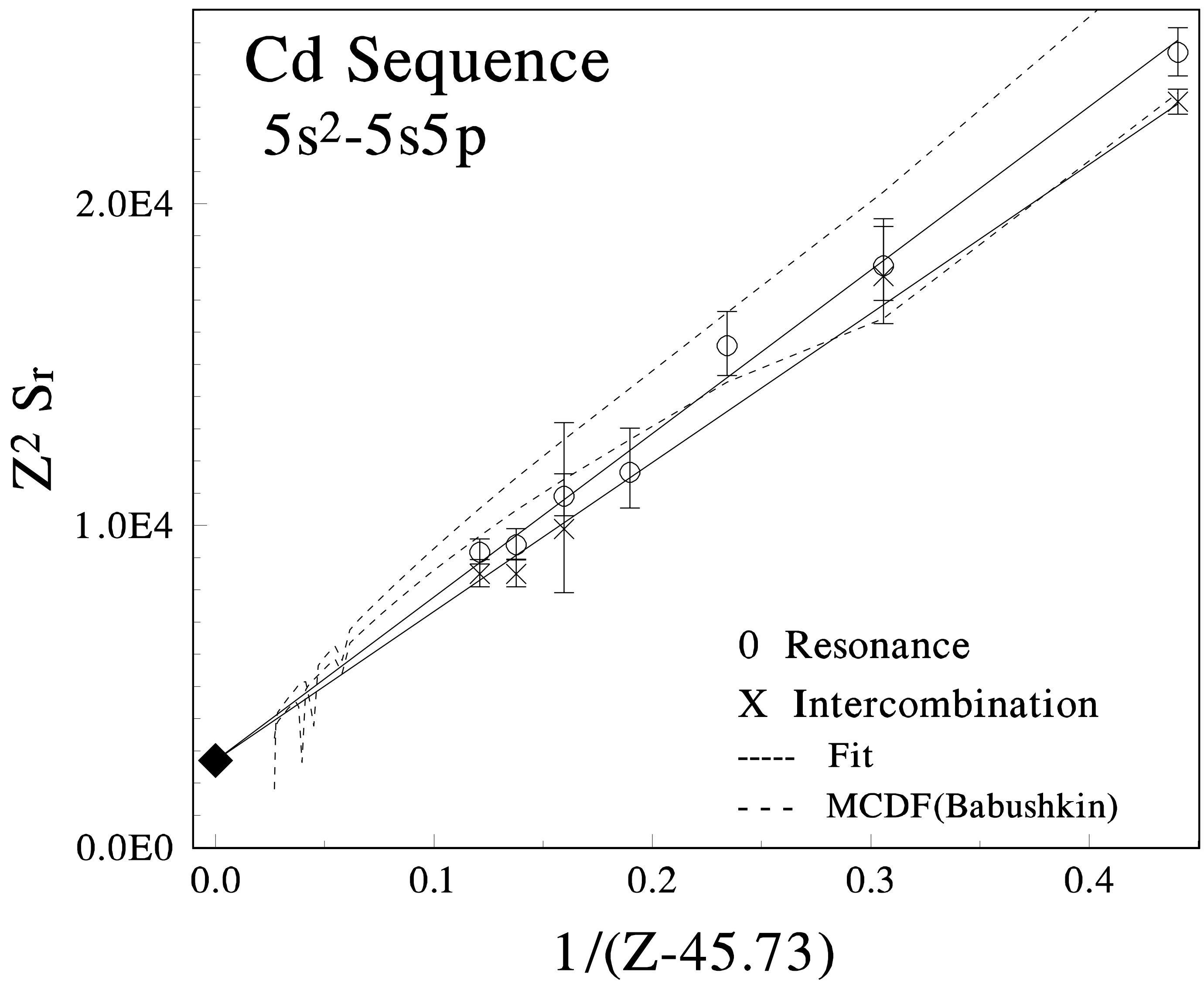

Cd Sequence
5s2-5s5p
2.0E4
1.0E4
0.0E0
Z2 Sr
0.0
0.1
0.2
0.3
0.4
1/(Z-45.73)
0 Resonance
X Intercombination
----- Fit
- - - MCDF(Babushkin)

Energies relative to $4d^{10}5s\ ^2S_{1/2}$
valence correlation only

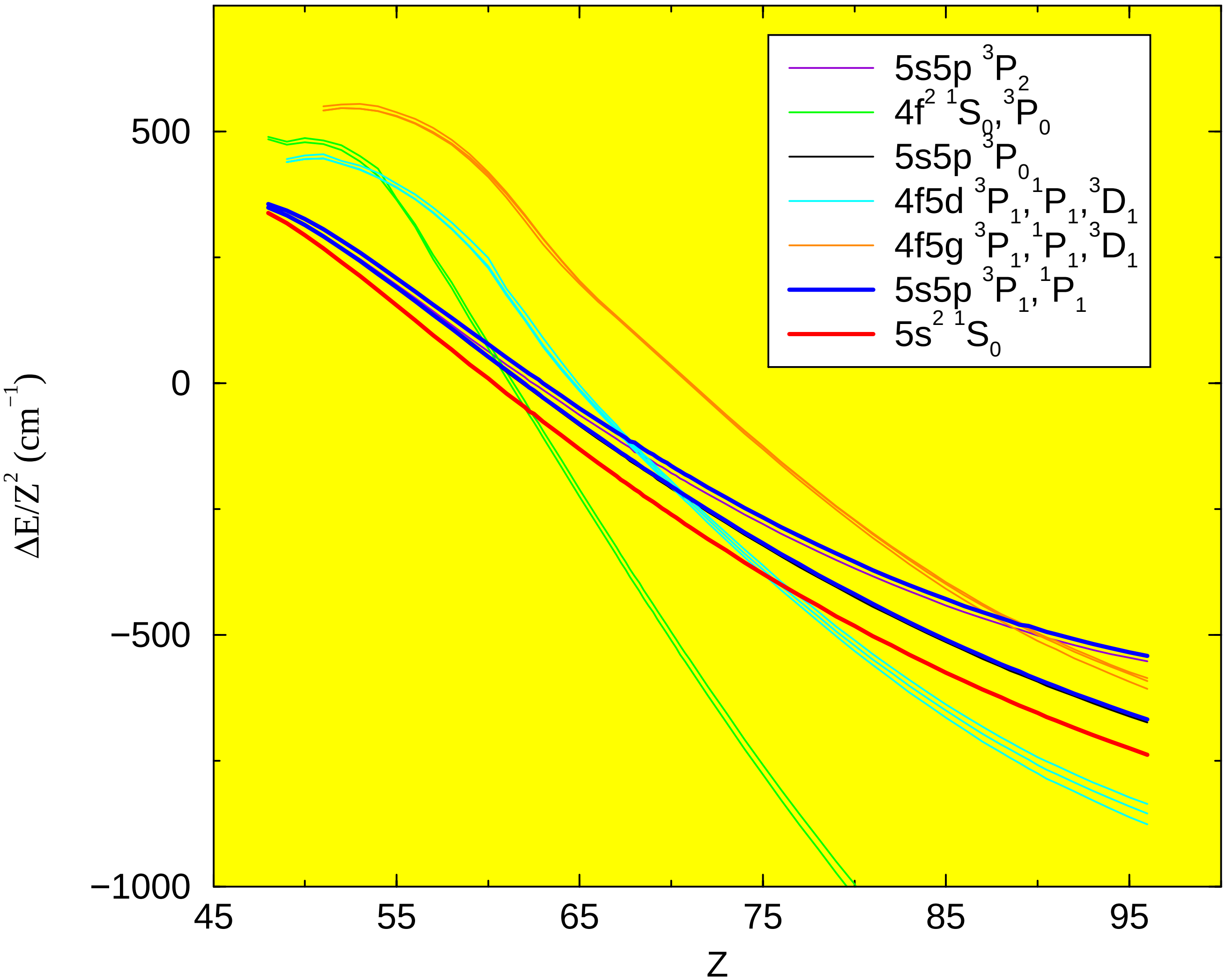

Many more cross–ings occur in the CV+V calculation at high Z, as the f correlation orbital becomes the spectroscopic 4f orbital in CSF's such as

$4d^9 4f\ 5\{s,p,d\}\ nl$

$4d^9 4f^2 5\{s,p,d\}$

TABLE III. Results for the intercombination transition $5s^2\ ^1S_0-5s5p\ ^3P_1$. Parentheses indicate quoted uncertainties in the experimental values as propagated from Table I.

		A_{ik} (ns^{-1})					
			MCDHF[a]		MCDHF[b]		
Z ion	λ (Å)	Expt.	Coulomb	Babushkin	Coulomb	Babushkin	SE[c]
48 Cd	3262	0.000418(7)	0.000348	0.000343	0.000449	0.000356	0.000419
49 In	2307	0.0023(2)	0.00212	0.00197	0.00244	0.00210	0.00210
50 Sn	1812		0.00676	0.00606	0.00701	0.00649	0.00614
51 Sb	1499		0.0154	0.0142	0.0158	0.0147	0.0137
52 Te	1282	0.025(6)	0.0304	0.0279	0.0310	0.0290	0.0261
53 I	1120	0.041(2)	0.0535	0.0490	0.0539	0.0509	0.0445
54 Xe	966	0.071(4)	0.0862	0.0793	0.0868	0.0822	0.0702
55 Cs	896		0.132	0.120	0.131	0.125	0.104
56 Ba	814		0.189	0.175	0.189	0.180	0.148
57 La	746		0.256	0.256	0.263	0.251	0.202
58 Ce	688				0.352	0.337	0.268
59 Pr	637				0.460	0.441	0.346
60 Nd	593				0.586	0.563	0.439
61 Pm	554				0.730	0.705	0.547
62 Sm	518				0.866	0.860	0.677
63 Eu	494				0.789	0.869	0.781
64 Gd	465				1.17	1.21	0.950
65 Tb	439				1.45	1.45	1.12
66 Dy	417				1.73	1.70	1.31
67 Ho	401				2.04	1.96	1.47

[a]Biémont *et al.* [15].
[b]This work, theoretical.
[c]This work, semiempirical, from fits shown in Figs. 3 and 4 and Eqs. (21) and (22).

sition data could be effectively linearized by the same value of C. Therefore the fits, subject to constraints $S_0=2700$ and $C(\mathrm{Res})=C(\mathrm{Int})$, yielded $C=45.73$, $B(\mathrm{Res})=50709$, and $B(\mathrm{Int})=46274$. Summarizing, the predicted line strengths can be specified by

$$S(\mathrm{Res})=\left(2700+\frac{50\,709}{Z-45.73}\right)\left(\frac{\cos\theta}{Z}\right)^2, \quad (20)$$

$$S(\mathrm{Int})=\left(2700+\frac{46\,274}{Z-45.73}\right)\left(\frac{\sin\theta}{Z}\right)^2, \quad (21)$$

$$\cot 2\theta=0.298+16.628/(Z-46.41). \quad (22)$$

The fitting constants can subsequently be sharpened as additional lifetime and energy level measurements become available. However it is significant to note that Eqs. (20)–(22) summarize, in very economical form, all of the information that is presently known concerning the line strengths of these Cd-like transitions.

The resonance and intercombination transition probability rates predicted by this semiempirical linearization are tabulated in Tables II and III for $48\leq Z\leq 67$, together with the wavelengths and the MCDHF calculations. For $Z>50$, the results of the present calculation agree with the predictions of the considerably more elaborate theoretical model of Ref. [15]. This agreement indicates that the present approach should be sufficient to characterize the isoelectronic trends predicted by the MCDHF method at intermediate values of Z; that is, away from the neutral-Z region that is complicated by extensive electron correlation effects, not yet in the high-Z region that is complicated by configuration interaction resulting from level crossings due to the contraction of the $4f$ shell. Although the quantitative description of the high-Z region would require a considerably more thorough theoretical effort, sharp deviations of our theoretical results from the smooth semiempirical isoelectronic trend in the high-Z region indicate the possible breakdown of the semiempirical formulation based on the single-configuration approach.

VI. CONCLUSIONS

The approximate linearities observed in the measured data through their expositions as $\cot 2\theta$ and Z^2S_r vs $1/(Z-C)$ (with C optimally chosen) have been verified for the Cd sequence by MCDHF calculations in the region $48\leq Z\leq 67$. This confirms the suggestion [4] that a few accurate lifetime measurements for the $5s5p\ ^1P_1$ and $5s5p\ ^3P_1$ levels can be

Contrast Cd and Mg Isoelectronic Sequences

Cd: ***48 electrons***
theoretically challenging
midrange Z, many stable isoelectronic ions

Hg: ***80 electrons***
very complex
only four radioactively stable ions

Cd: Plunging levels from unfilled 4f subshell
perturb 5s5p for certain $Z \geq 60$ ions
eventually replace $5s^2$ as ground state

Hg: $6s^2$ and 6s6p remain below levels from 5f and 5g through $Z = 92$

$6s^2$-6s6p rates in radioactive elements difficult to measure, but may dominate radiative transfer in plasmas that contain these ions.

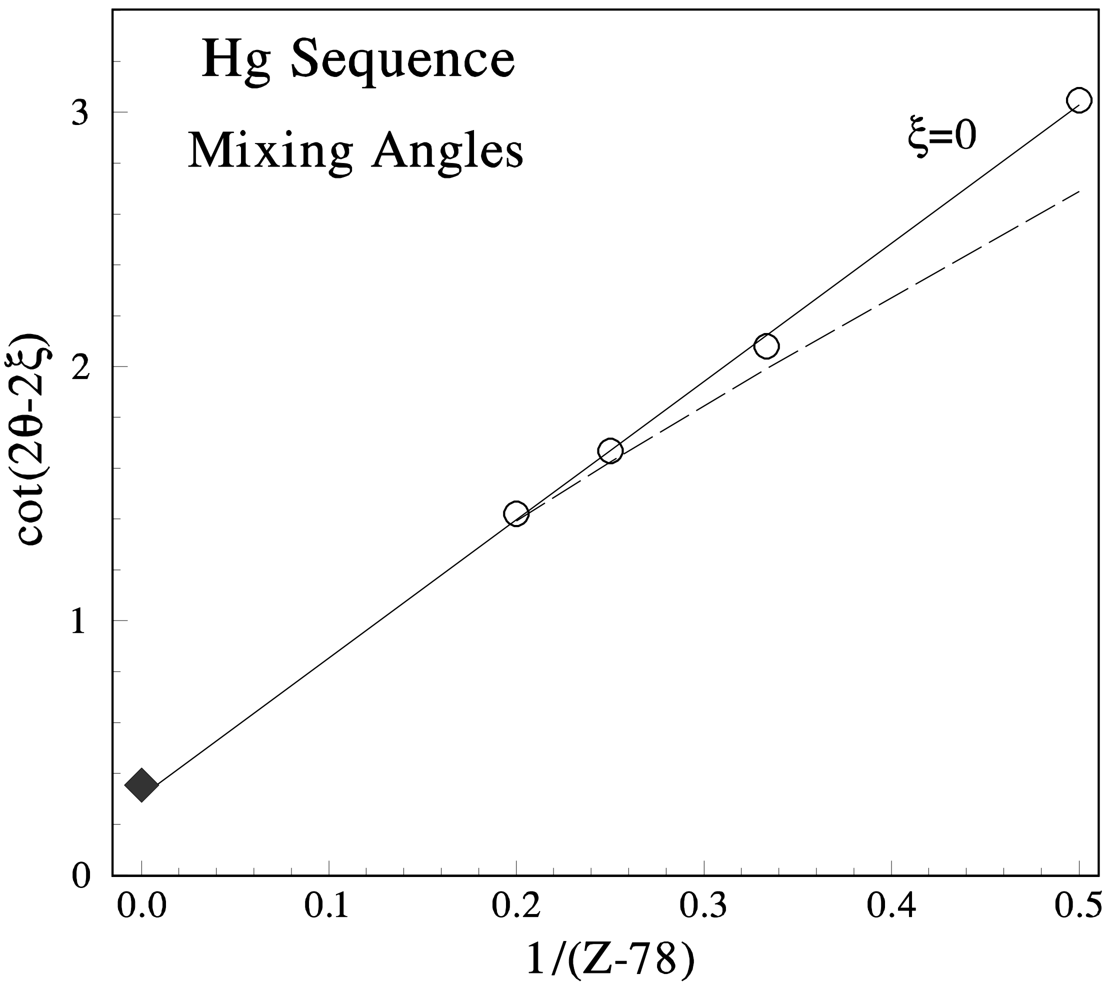
Hg Sequence
Mixing Angles
ξ=0
cot(2θ-2ξ)
1/(Z-78)
0
1
2
3
0.0
0.1
0.2
0.3
0.4
0.5

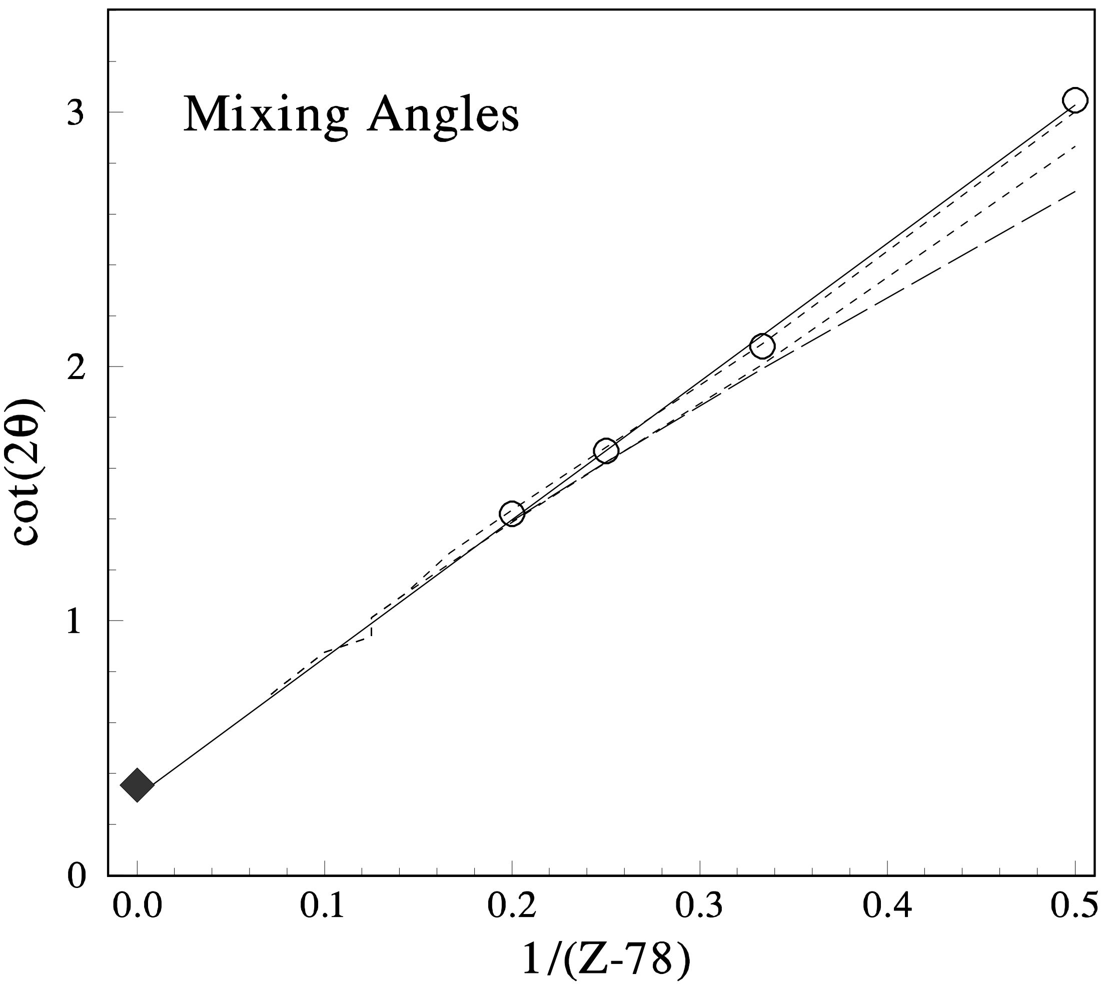

Mixing Angles
cot(2θ)
1/(Z-78)
0
1
2
3
0.0
0.1
0.2
0.3
0.4
0.5

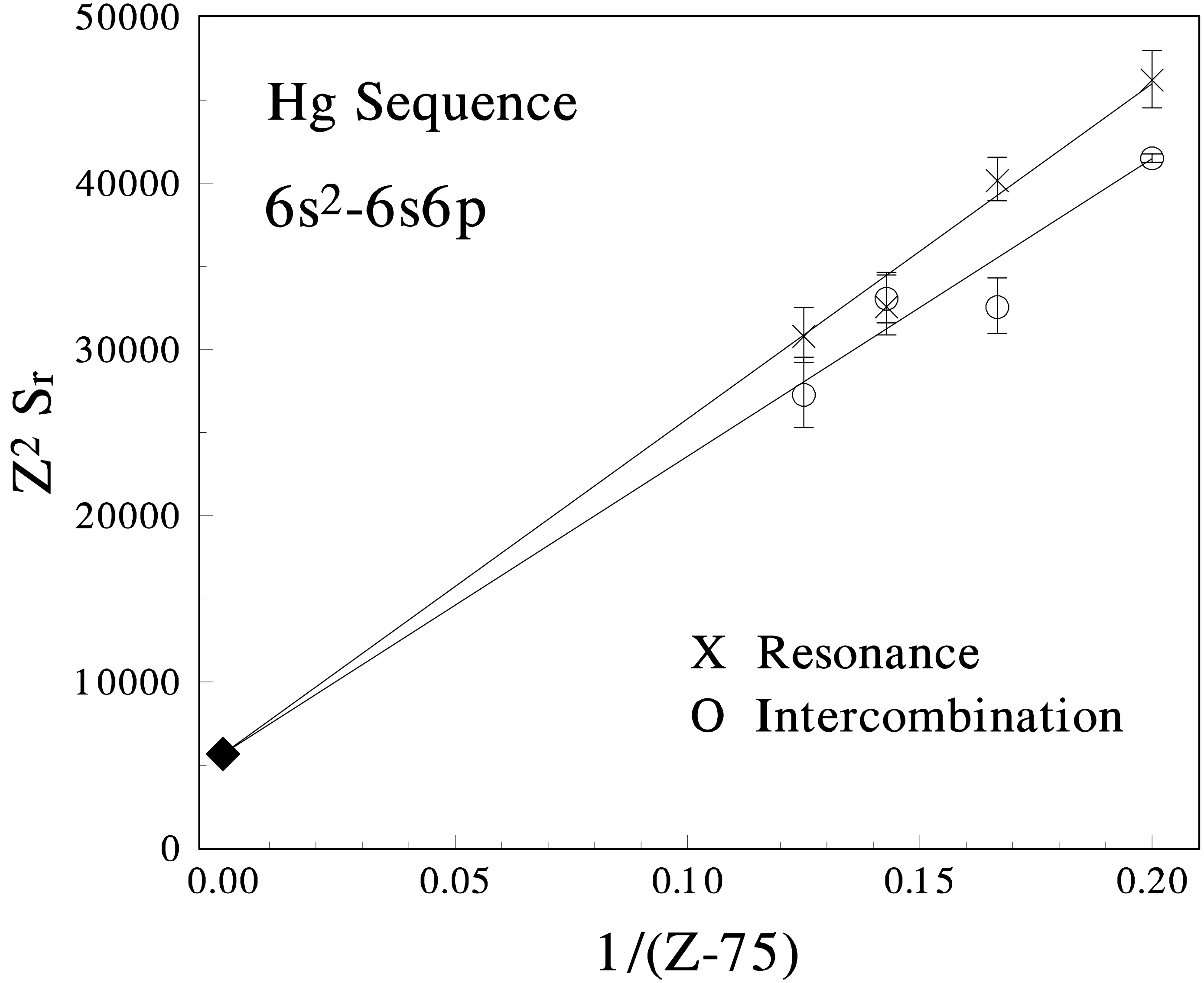

Hg Sequence
6s2-6s6p
X Resonance
O Intercombination
50000
40000
30000
20000
10000
0
0.00
0.05
0.10
0.15
0.20
Z2 Sr
1/(Z-75)

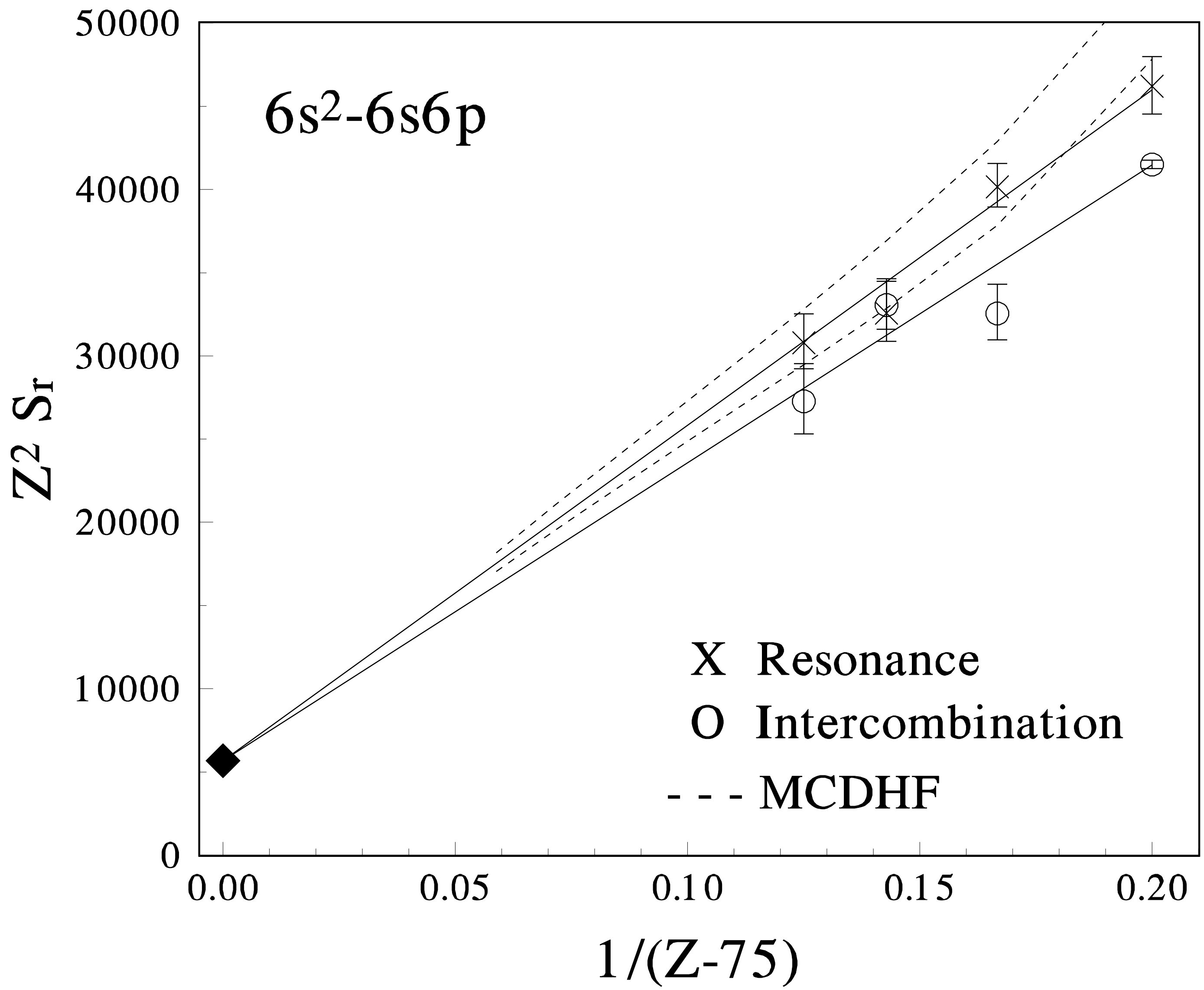

6s^2-6s6p
$Z^2\ S_r$
1/(Z-75)
X Resonance
O Intercombination
- - - MCDHF
50000
40000
30000
20000
10000
0
0.00
0.05
0.10
0.15
0.20

TABLE IV: Lifetime predictions. Parentheses denote quoted or propagated uncertainties.

Z	Ion	Resonance: λ_R(Å)[a]	Resonance: τ_R(ns) Expt.[c]	Resonance: τ_R(ns) SE[d]	Resonance: τ_R(ns) MCDHF[e]	Intercombination: λ_I(Å)[a]	Intercombination: τ_I(ns) Expt.[c]	Intercombination: τ_I(ns) SE[f]	Intercombination: τ_I(ns) MCDHF[e]	$\sin(\theta\text{-}\xi)$[b]
80	Hg I	1849.5	1.3[illegible](5)[a]	1.346	1.066	2537.3	118.9(4)[b]	117.9	123.5	0.1771
81	Tl II	1321.7	0.[illegible](4)[c]	0.682	0.543	1908.7	39(3)[c]	36.9	36.0	0.2307
82	Pb III	1048.9	0.309(21)[d]	0.360	0.334	1553.0	15.2(7)[f]	16.1	16.0	0.2725
83	Bi IV	872.6	0.249(13)[e]	0.243	0.228	1317.1	9.1(7)[g]	8.62	8.76	0.3065
84	Po V	746.0		0.176	0.166	1146.3		5.27	5.44	0.3417
85	At VI	653.2		0.133	0.125	1019.4		3.56	3.68	0.3675
86	Rn VII	578.5		0.104	0.0979	919.9		2.57	2.65	0.3889
87	Fr VIII	517.6		0.0829	0.0781	839.2		1.94	2.00	0.4070
88	Ra IX	466.9		0.0671	0.0633	772.0		1.52	1.56	0.4223
89	Ac X	424.0		0.0550	0.0520	715.7		1.23	1.25	0.4355
90	Th XI	387.1		0.0455	0.0432	667.4		1.01	1.03	0.4469
91	Pa XII	355.0		0.0380	0.0362	625.5		0.853	0.865	0.4569
92	U XIII	326.8		0.0319	0.0305	588.7		0.728	0.736	0.4656

[a] MCDHF values from Table I for $Z \geq 84$.
[b] Extrapolates for $Z \geq 84$ using Eq. 12, 13.
[c] Recommended values from Table IV.
[d] Semiempirical values from Eqs. 10, 12, 13.
[e] MCDHF values from this work.
[f] Semiempirical values from Eqs. 11, 12, 13.

$$Z^2 S_r(Res) = 5670[1 + 35.55/(Z - 75)]$$

$$Z^2 S_r(Int) = 5670[1 + 31.57/(Z - 75)]$$

$$\cot 2\theta = 0.3096 + 5.437/(Z - 78)$$

$$R_{12}/R_{11} = 0.9931 - 0.0334/(Z - 79)^{1.6}.$$

Dirac Formulation

For ns^2-$nsnp$ there are two radial wavefunctions $R_{2j,2j'}$

$$S(Res) \propto [R_{11}\cos(\theta_{jj}-\theta) - R_{31}\sin(\theta_{jj}-\theta)]^2$$

$$S(Int) \propto [R_{11}\sin(\theta_{jj}-\theta) + R_{31}\cos(\theta_{jj}-\theta)]^2$$

and the jj coupling limit

$$\tan\theta_{jj} = \sqrt{\tfrac{1}{2}}$$

reduces by trigonometric identities to

$$S_r(Res) \equiv \frac{S(Res)}{\cos^2(\theta-\xi)}$$

$$S_r(Int) \equiv \frac{S(Int)}{\sin^2(\theta-\xi)}$$

where

$$\tan\xi \equiv \sqrt{2}\frac{R_{31}-R_{11}}{2R_{31}+R_{11}}.$$

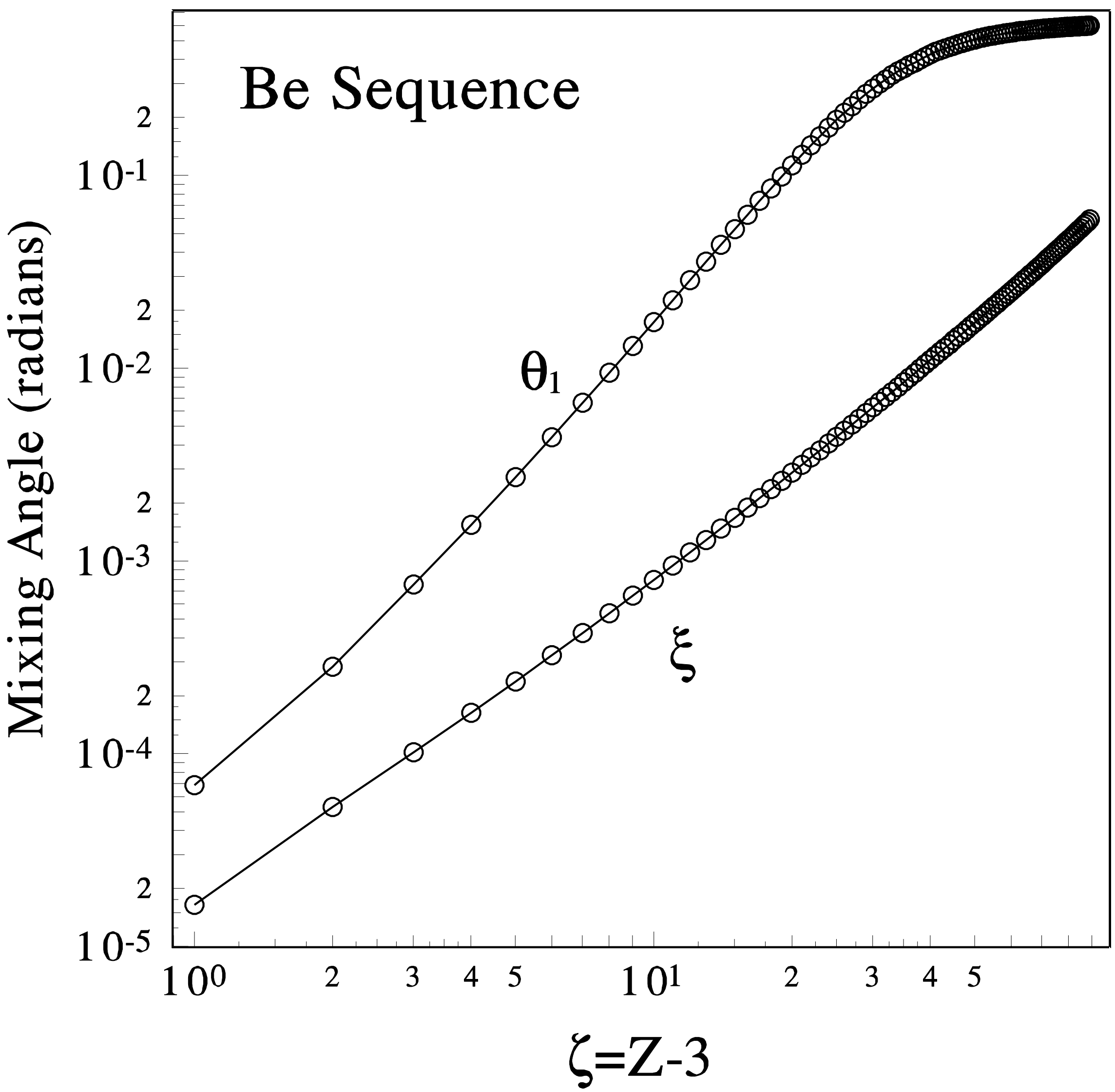
Be Sequence
Mixing Angle (radians)
θ1
ξ
ζ=Z-3
10-1
10-2
10-3
10-4
10-5
100
101
2
3
4
5

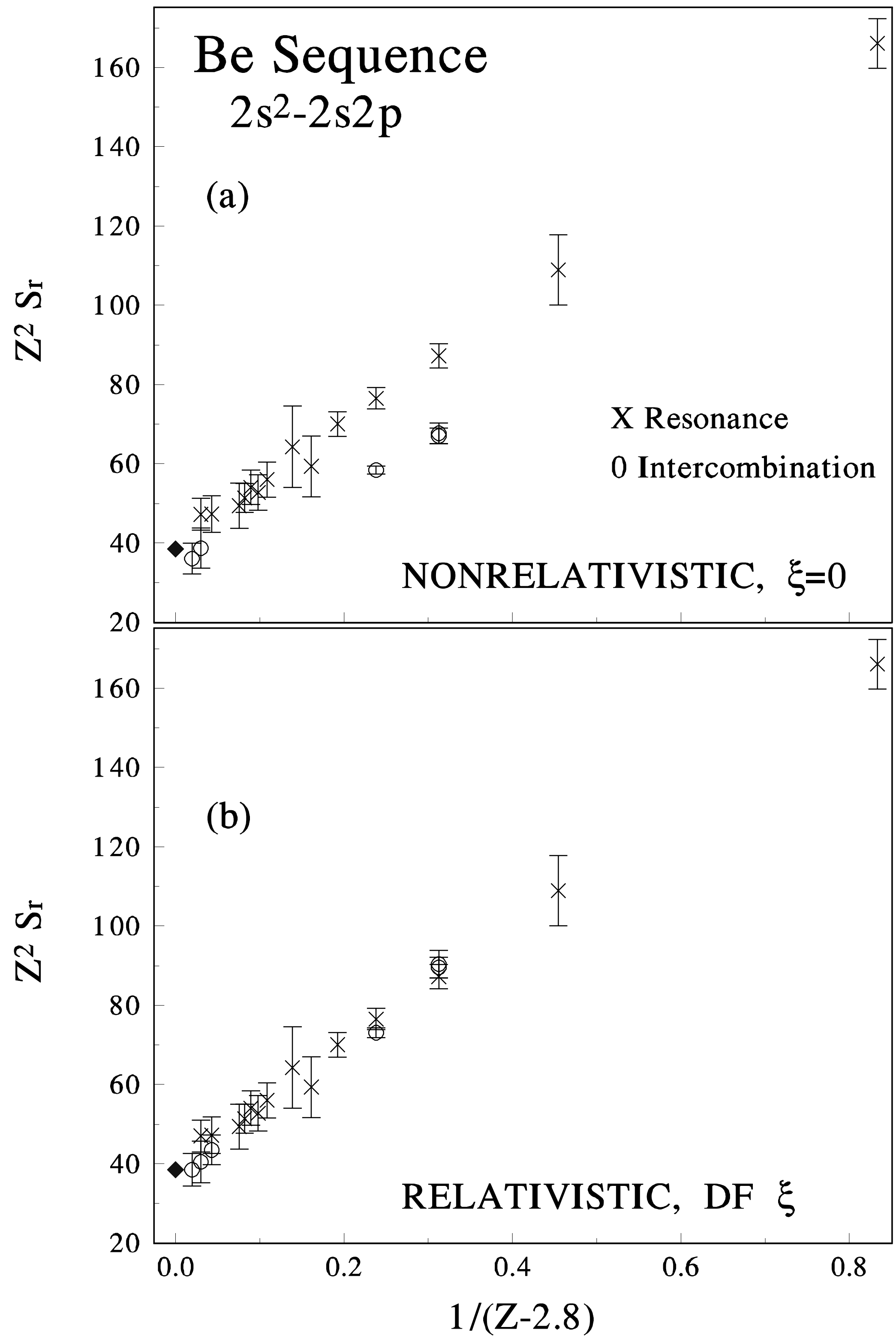
Be Sequence
$2s^2$-2s2p
(a)
X Resonance
0 Intercombination
NONRELATIVISTIC, ξ=0
(b)
RELATIVISTIC, DF ξ
Z^2 S_r
1/(Z-2.8)

IC 2s2p ϑ

C.I. $2s^2$, $2p^2$ ϕ

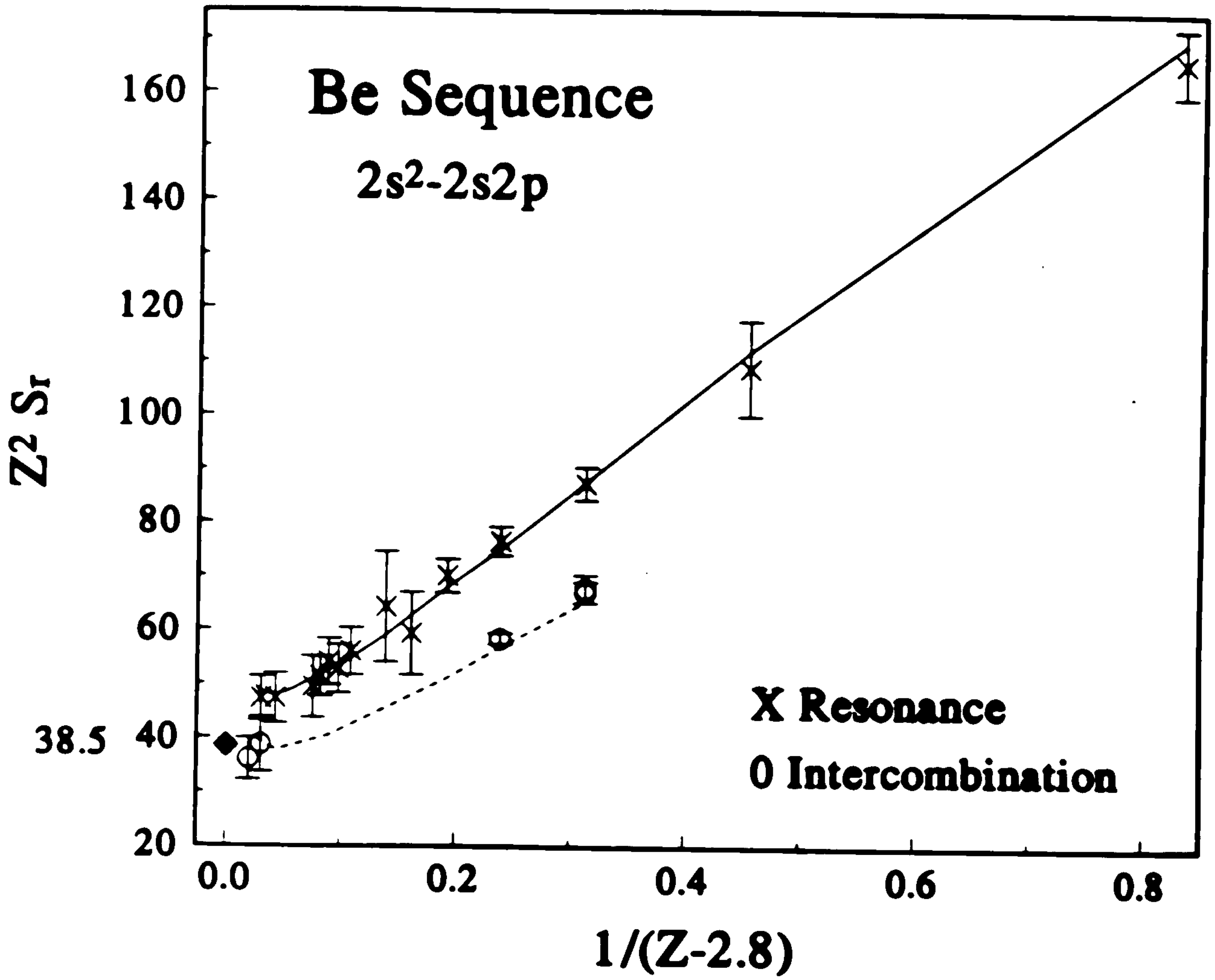

$$S_H' = \frac{2}{3}\left(\sqrt{3}\cos\phi - \sin\phi\right)^2 S_H \xrightarrow[\phi \cong 13^\circ]{S_H = 54} 38.5$$

—— Fleming et al, Phys. Scr 53, 446 (1996)

- - - Ynnerman & Froese Fischer, PR A 51, 2020 (1995)

CLOSED SHELL CORES WITH HYDROGENIC ORDERING

$$N_e = 2\sum_{n=1}^{n_{max}} n^2 = \frac{2}{3} n_m (n_m + \tfrac{1}{2})(n_m + 1)$$

$$= 2(1 + 4 + 9 + 16 + \cdots)$$

$\underbrace{2(1}_{2}$ (He-like)

$\underbrace{2(1+4}_{10}$ (Ne-like)

$\underbrace{2(1+4+9}_{28}$ (Ni-like)

$\underbrace{2(1+4+9+16}_{60}$ (Nd-like)

Promethium Isoelectronic Sequence

$N_e = 61$

hyper-alkalilike for large Z

Samarium Isoelectronic Sequence

$N_e = 62$

hyper-alkaline-earthlike Sequence

He
Ne
Ni
Nd

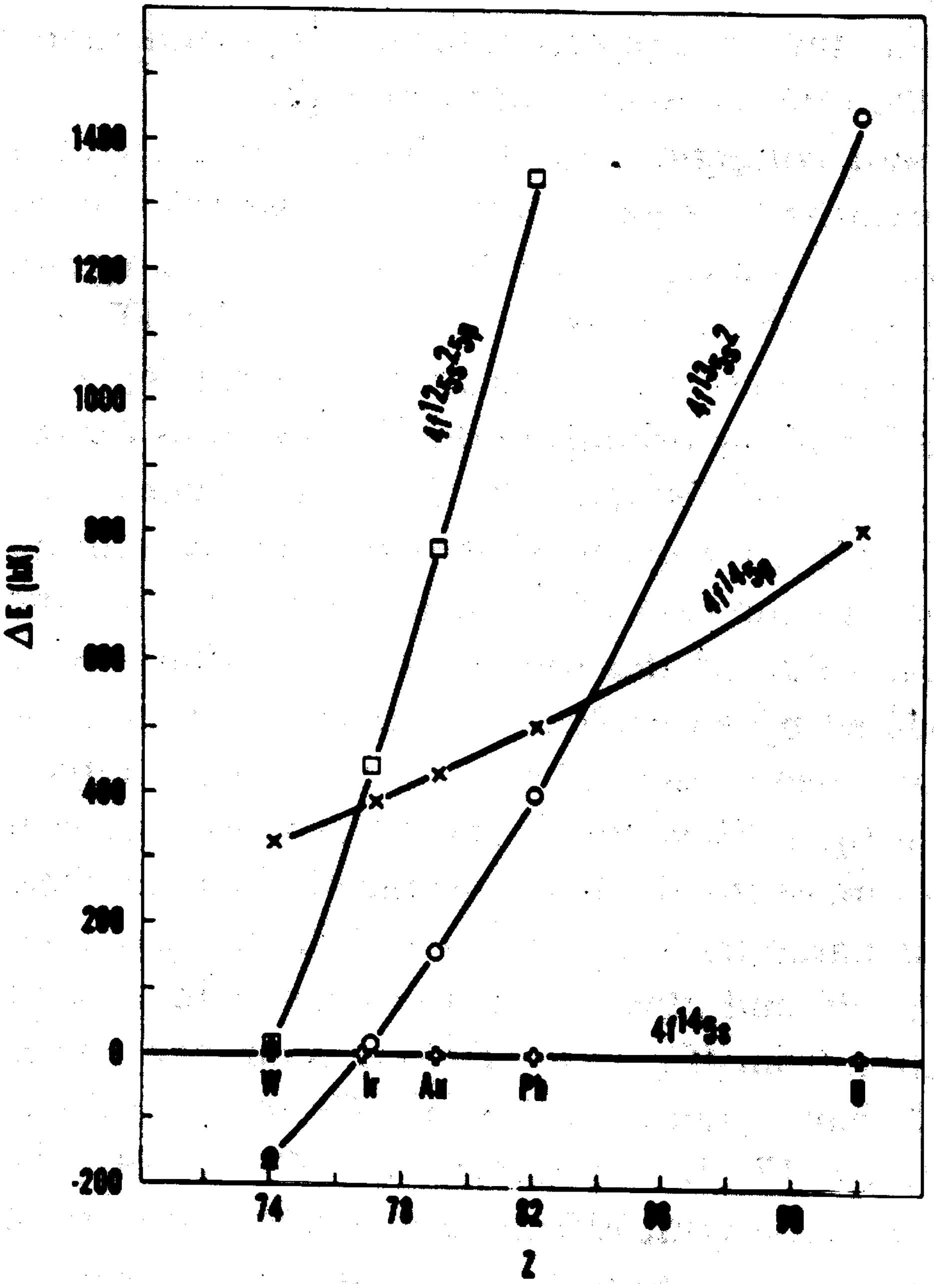

Fig. 1. Upper promethium sequence. The average energies of the indicated configurations ($4f^{14}5p$, $4f^{13}5s^2$, $4f^{12}5s^25p$), relative to that of $4f^{14}5s$, are plotted against nuclear charge. Included are both the Hartree–Fock energy (HF) and its lowest-order relativistic correction (Pauli). Also plotted for W^{+13} are the relativistic Hartee–Fock (HFR) results of Cowan [5] indicated by triangles. Other symbols indicate results of the present work. Energies are given in units of 10^3 cm^{-1} (kK).

EUV-spectra from tungsten Pm-like W^{13+}

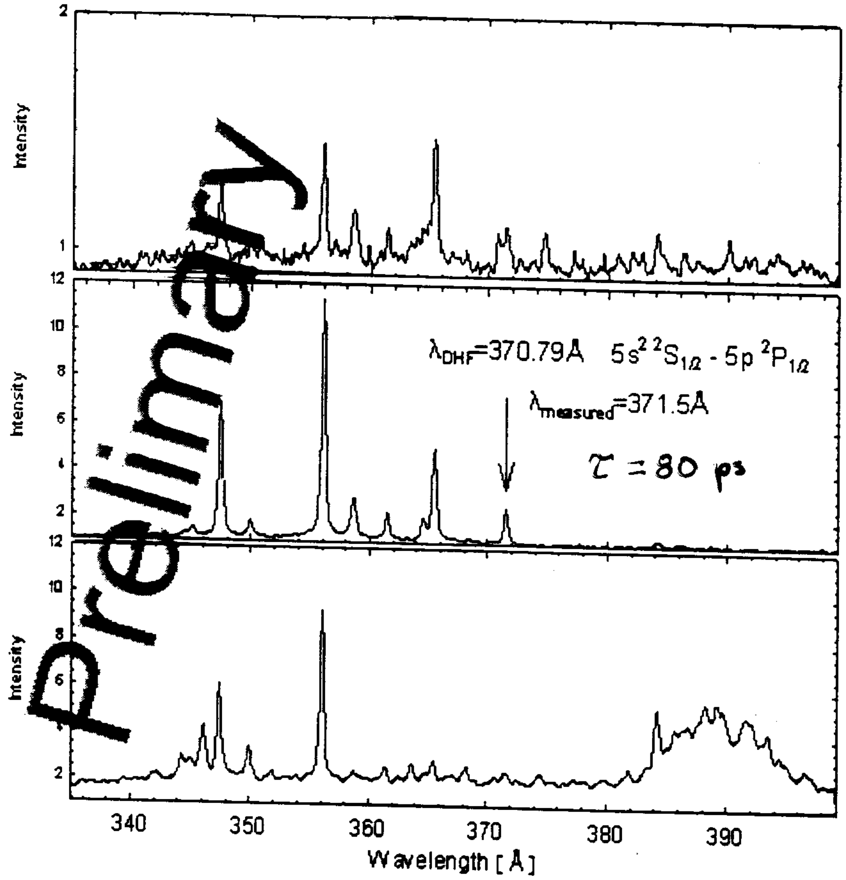

g1018001 V_{drift}= 0.4000 kV
Y=410
electron beam energy 0.417 keV
electron beam current 10 mA
no dump of trap
data acquisition 60 min
grating 600 l/mm; 3.5 blaze
slit 18 μm

g1018004
Y = 410
V_{drift}= 0.3053 kV
electron beam energy 0.311 keV
electron beam current 10 mA
60 min

g1018005
Y = 410
V_{drift}= 0.2494 kV
electron beam energy 0.244 keV
electron beam current 10 mA
60 min

Sm seq		
Res	249 Å	21 ps
Int	423 Å	752 ps

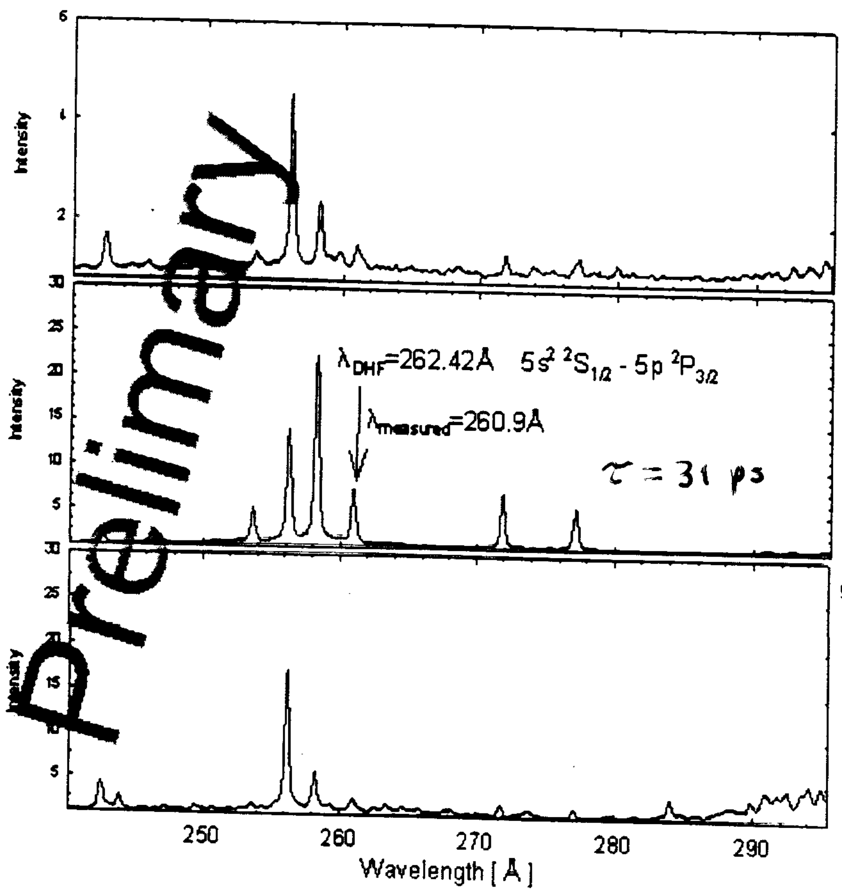

g1018002
Y = 348
V_{drift}= 0.4000 kV
electron beam energy 0.417 keV
electron beam current 10 mA
60 min

g1018003
Y = 348
V_{drift}= 0.3053 kV
electron beam energy 0.311 keV
electron beam current 10 mA
ca. 40 min

g1018007
Y = 348
V_{drift}= 0.2475 kV
electron beam energy 0.242 k
electron beam current 10 m
30 min

Projection within 385+-250pixe
calib. Sep2000

SAMARIUM SEQUENCE

Z Ion	$({}^1S_0 - {}^1P_1)$ λ(Å) MCDF	τ(ps) MCDF	τ(ps) Mix	$({}^1S_0 - {}^3P_1)$ λ(Å) MCDF	λ(Å) Obs	τ(ps) MCDF	τ(ps) Mix	τ(ps) HF/CI	τ(ps) Obs
74	249.3	20.7		423.3		752			
75 Re	237.5	17.4	11.9	398.4		608	393		
76 Os	221.3	12.8	10.3	376.2	[366.3]	502	333	281	
77 Ir	207.0	11.1	9.0	356.3	[347.0]	421	285	240	[260]
78 Pt	193.9	9.7	8.1	338.3	[330.0]	357	248	207	[200]
79 Au	182.0	8.6	7.3	321.8	[313.6]	307	219	180	[170]
80 Hg	171.0	7.5	6.5	306.8		266	194		
81 Tl	160.9	6.7	5.8	293.1		232	172		
82 Pb	151.5	5.9	5.1	280.4		205	153		
83 Bi	142.8	5.2	4.5	268.7		182	136		
84 Po	134.7	4.6	4.0	257.8		162	120		
85 At	127.2	4.1	3.5	247.7		146	107		
86 Rn	120.2	3.7	3.1	238.2		132	95		
87 Fr	113.6	3.3	2.8	229.4		119	86		
88 Ra	107.5	2.9	2.5	221.2		109	79		
89 Lu	101.8	2.6	2.2	213.4		100	74		
90 Th	96.4	2.3	2.1	206.1		92	71		
91 Pa	91.3	2.1	2.0	199.3		84	70		
92 U	86.6	1.8	1.9	192.8		78	71		

MCDF: Curtis, JOSA B3, 1102 (1986); Grant-2 program.
Mix : Singlet-Triplet mixing with Pm line strengths.
Pm from Curtis & Ellis, PRL 45, 2099 (1980); MCHF+BP.
HF/CI: Kaufman (person communication); Cowan code.
Obs: Kaufman, Heckmann, Träbert, Möller, Lodwig & Blank ~~(personal communication)~~. Phys. Scr. 42, 705 (1990).

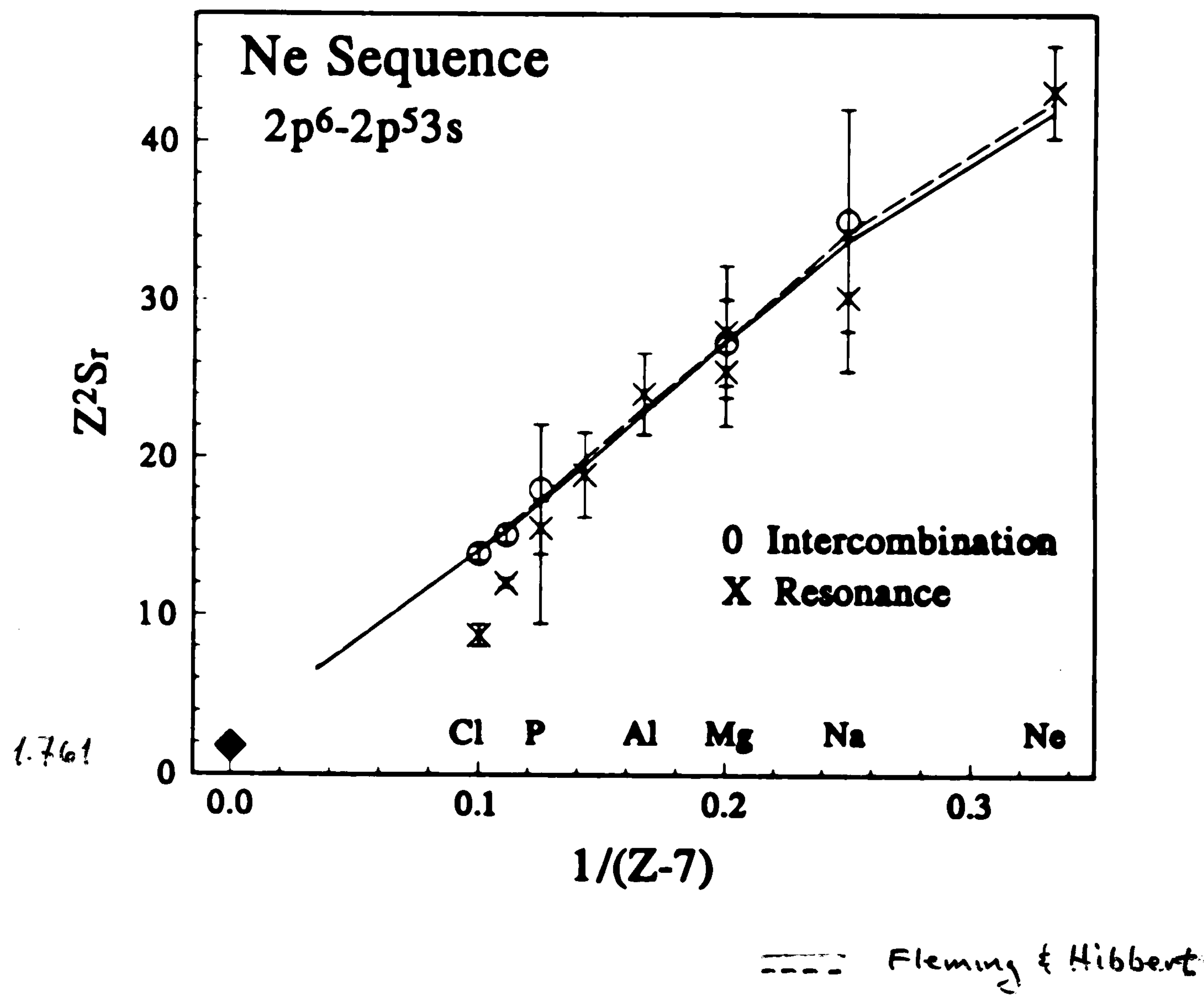
Ne Sequence
$2p^6$-$2p^5 3s$
0 Intercombination
X Resonance
Cl
P
Al
Mg
Na
Ne
$Z^2 S_r$
1/(Z-7)
0
10
20
30
40
0.0
0.1
0.2
0.3
1.761
Fleming & Hibbert

TABLE III. Ne sequence $2p^5 3s\ ^{1,3}P$ levels (lifetimes in ps).

Z	Ion	Intercombination transitions τ_{expt}	τ_{pred}	Resonance transitions τ_{expt}	τ_{pred}	$\sin\theta$
10	Ne	29600±1000,10[a,j]		1470±100[a]	1547	0.2656
		31700±1600,10[b,j]		1870±180,10[b,j]		
		29800±2000,10[c,j]		1300±100,10[c,j]		
11	Na	6000±1200[a]	5623	320^{+50}_{-40}[a]	346	0.2131
		10600±500,10[d,j]		580±60[d]		
12	Mg	1900±190[e]	1820	100±15[e]	131	0.2299
				110^{+15}_{-10}[a]		
13	Al		637	46^{+10}_{-5}[a]	63	0.2677
14	Si		248	28^{+8}_{-4}[a]	36	0.3171
15	P	130±30[a]	137	18^{+7}_{-2}[a]	21	0.3731
16	S	52±2[f]	52	14.5±1.0[g]	15	0.4309
		49±13[h,j]		12±3[h,j]		
17	Cl	27±1[f]	27	13±1[f]	11	0.4872
		34±12[h,j]		10±2[h,j]		
		30±5[i,j]		8±2[i,j]		
18	Ar	19±4[i,j]	16	6.5±2.0[i,j]		
34	Se		0.28		0.60	0.7847
35	Br		0.24		0.53	0.7878
36	Kr		0.21		0.47	0.7904
37	Rb		0.19		0.42	0.7927
38	Sr		0.16		0.38	0.7947
39	Y		0.14		0.34	0.7966

[a]This work.
[b]Lawrence and Liszt, Ref. [56].
[c]Kernahan *et al.*, Ref. [57].
[d]Schlagheck, Refs. [58,59].
[e]Buchet *et al.*, Ref. [60].
[f]Westerlind *et al.*, Ref. [61].
[g]Kirm *et al.*, Ref. [65].
[h]Gardner *et al.*, Ref. [62].
[i]Berry *et al.*, Ref. [63].
[j]Excluded from plot and fit.

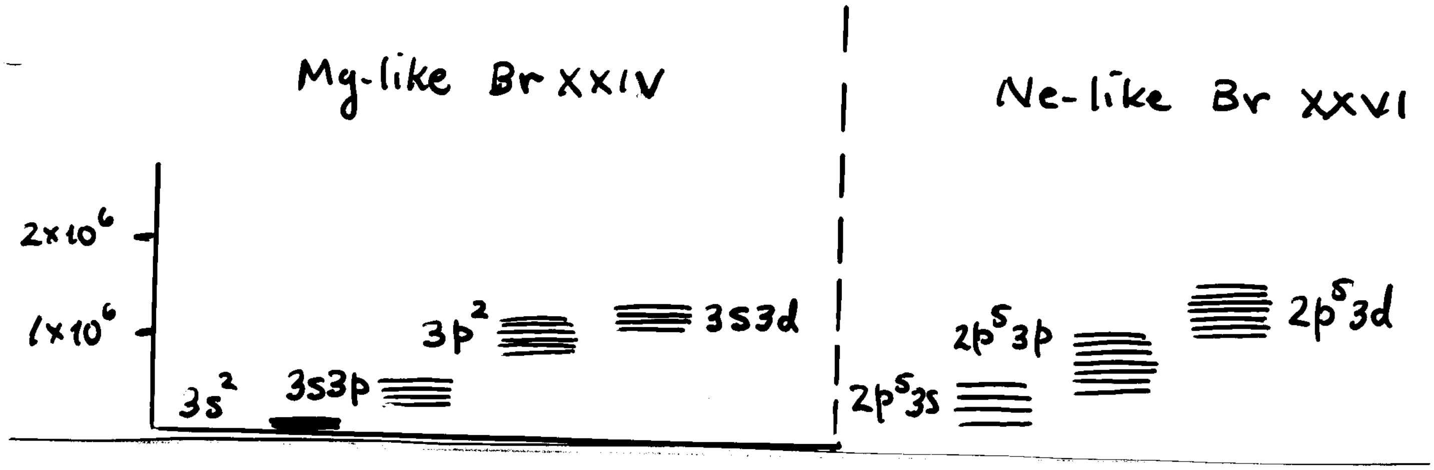
Mg-like Br XXIV
Ne-like Br XXVI
2x10^6
1x10^6
3s^2
3s3p
3p^2
3s3d
2p^5 3s
2p^5 3p
2p^5 3d

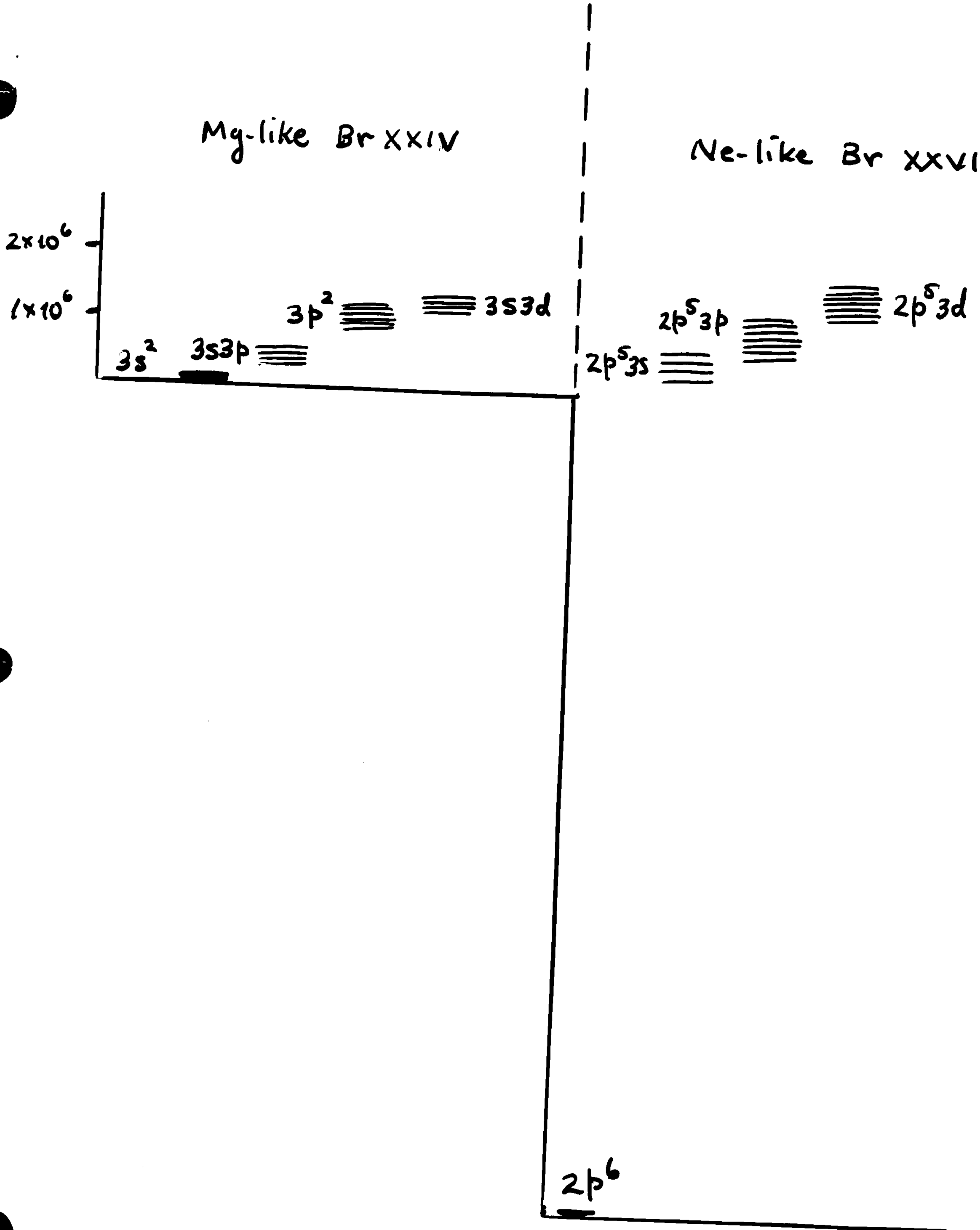
Mg-like Br XXIV
Ne-like Br XXVI
2×10⁶
1×10⁶
3s²
3s3p
3p²
3s3d
2p⁵3s
2p⁵3p
2p⁵3d
2p⁶

BRANCHING FRACTIONS FROM DIFFERENTIAL LIFETIME MEASUREMENTS

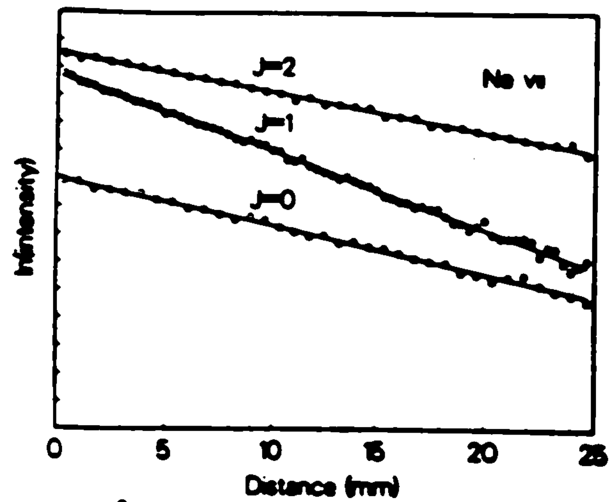

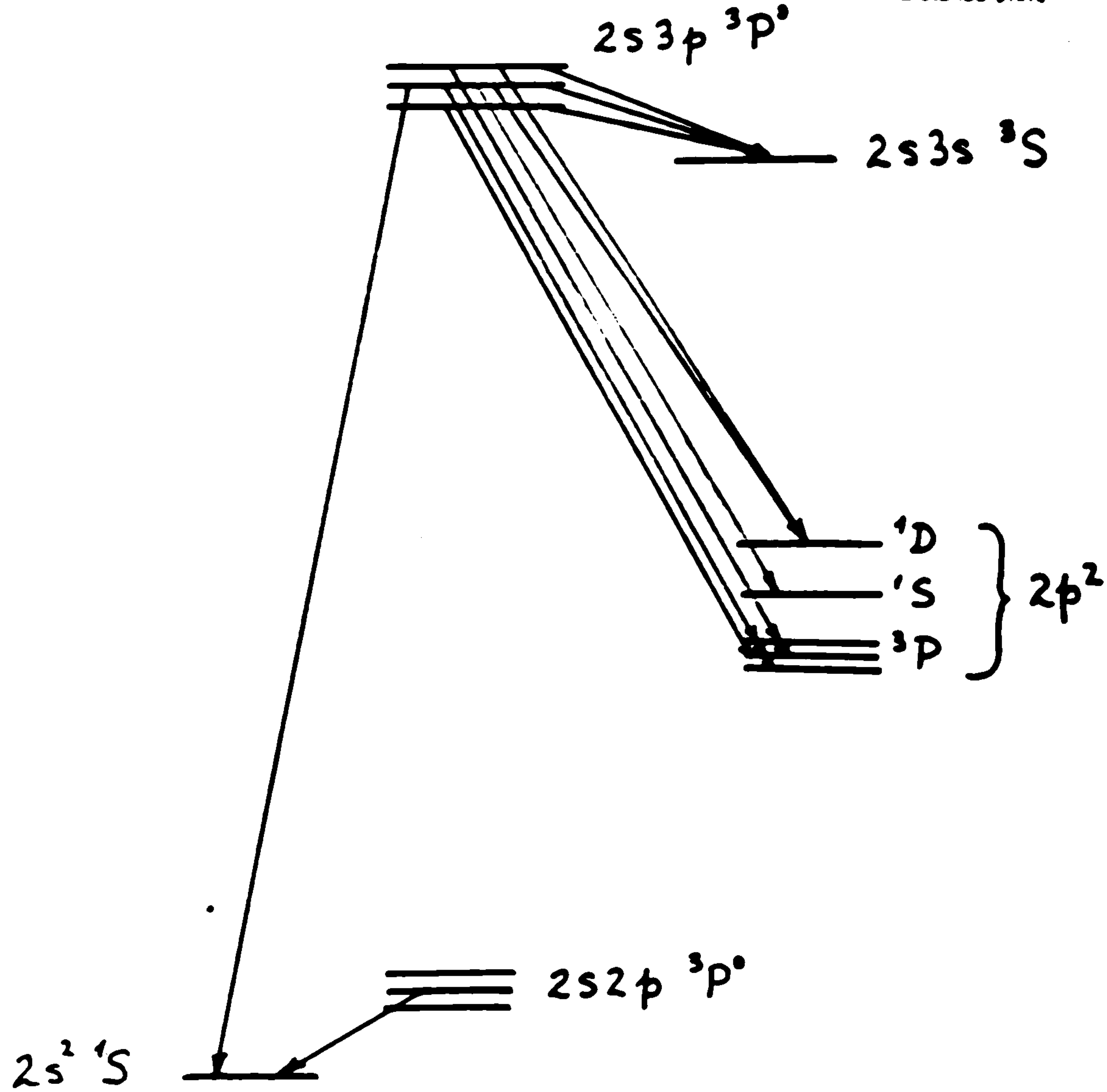

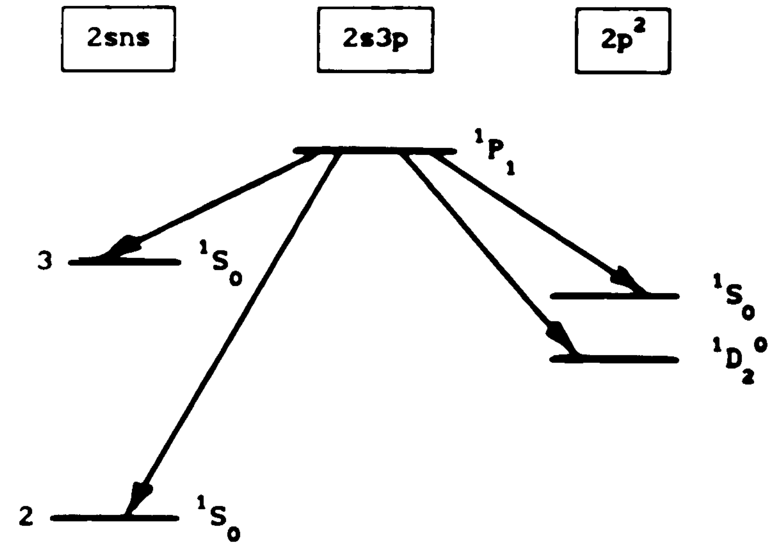

Branching Fractions (%)

2s3p $^1P_1$ →	$2s^2$ $^1S_0$	$2p^2$ $^1D_2$	$2p^2$ $^1S_0$	2s3s $^1S_1$
Be I	55.6	26.5	0.1	17.9
B II	68.6	14.4	13.9	3.0
C III	87.3	11.6	0.8	0.2
N IV	89.9	9.5	0.4	0.1
O V	91.4	8.2	0.3	0.05
Ne VII	93.5	6.3	0.2	0.02
Fe XXIII	95.9	3.1	0.1	0.01

Bhatia & Mason, A&A 103, 324 (1981) [Fe]

Laughlin *et al*, J.Phys.B 11, 2243 (1978) [Others]

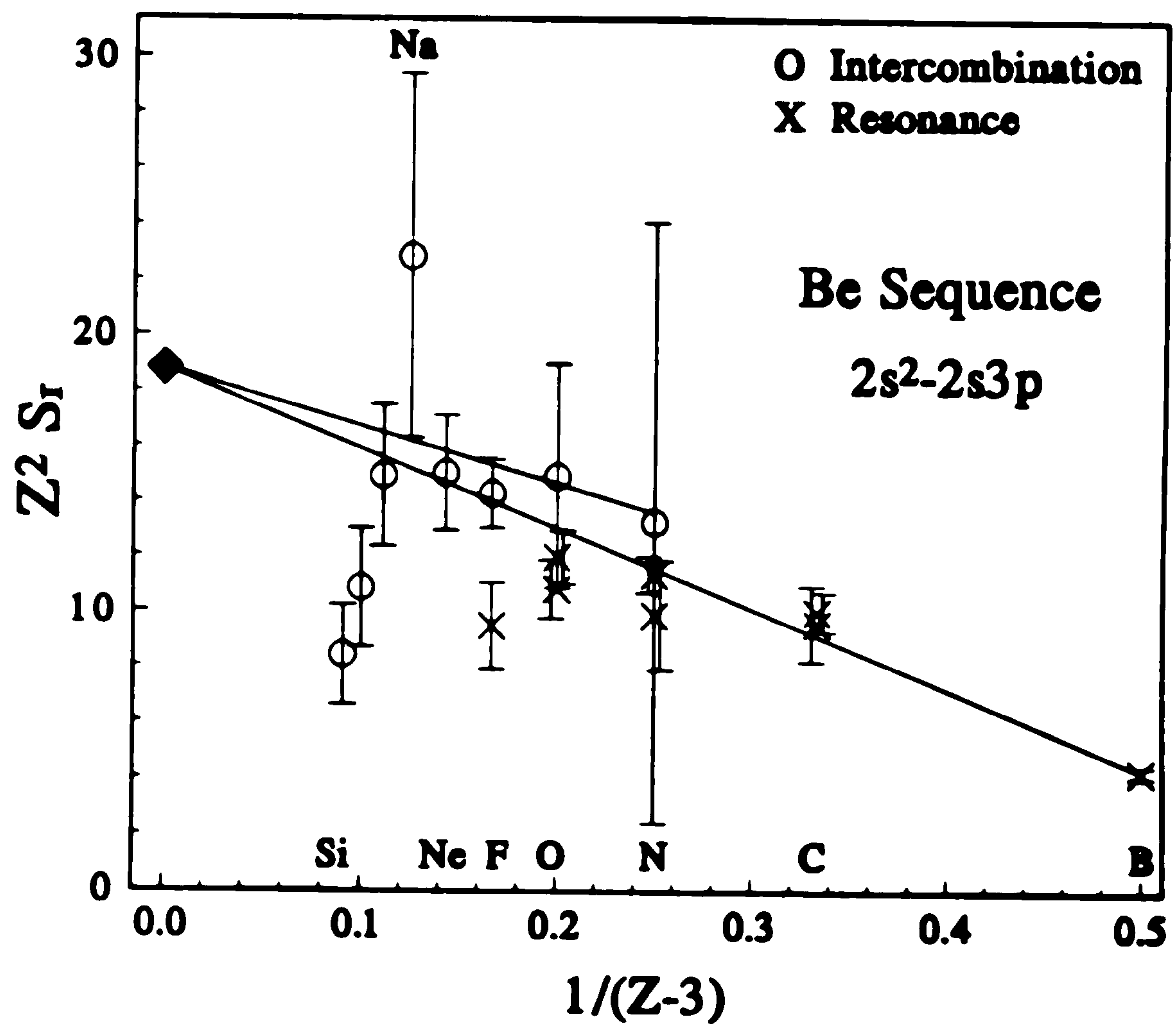

30
20
10
0
Na
O Intercombination
X Resonance
Be Sequence
2s²-2s3p
Z² S_r
Si
Ne
F
O
N
C
B
0.0
0.1
0.2
0.3
0.4
0.5
1/(Z-3)

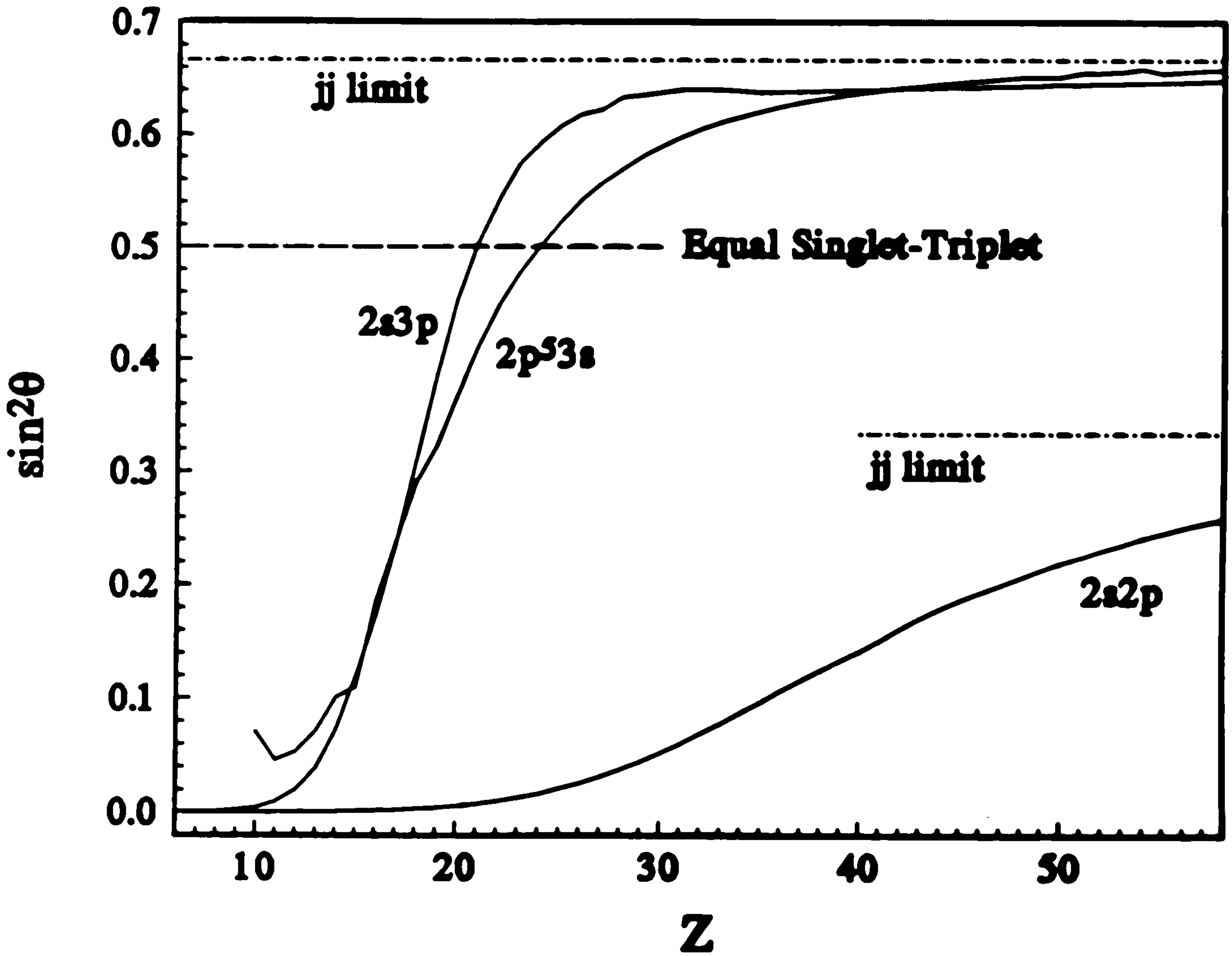

0.7
0.6
0.5
0.4
0.3
0.2
0.1
0.0
jj limit
Equal Singlet-Triplet
2s3p
$2p^53s$
jj limit
2s2p
10
20
30
40
50
Z
$\sin^2\theta$

TABLE II. Be sequence $2s3p\ ^{1,3}P$ levels (lifetimes in ns). The experimental uncertainty in the last figure is given in parentheses. Branching fractions without labels are interpolated.

		Intercombination transitions				Resonance transitions				
Z	Ion	$\tau_{2,0}$	τ_1	A_{expt}	A_{pred}	τ	BF	A_{expt}	A_{pred}	$\sin\theta$
5	B				0.0001	1.98(9)[a]	0.686[b]	0.346(16)	0.35	0.0199
6	C				0.0004	0.28(4)[c]	0.873[b]	3.12(45)	2.96	0.0113
						0.268(20)[d]		3.26(24)		
7	N	8.98(10)	8.72(12)	0.0033(20)[e]	0.0028	0.087(5)[c]	0.899[b]	10.3(6)	10.4	0.0164
						0.10(2)[f]		9(2)		
8	O	5.31(5)	4.74(7)	0.0228(4)[e]	0.019	0.041(4)[c]	0.914[b]	22(2)	26.5	0.0266
						0.037(3)[g]		25(2)		
9	F	2.94(3)	2.24(4)	0.102(9)[c]	0.100	0.024(4)[c]	0.927	30(6)	56.2	0.0419
10	Ne	1.75(7)	1.00(6)	0.43(6)[h]	0.418		0.934[b]		106	0.0627
11	Na	1.10(16)	0.29(6)	2.54(73)[i]	1.08		0.930		180	0.0960
12	Mg	0.745(60)	0.145(20)	5.55(96)[i]	5.78		0.943		296	0.1400
13	Al	0.515(50)	0.071(12)	12.1(24)[i]	17.6		0.946		430	0.1980
14	Si	0.365(25)	0.036(7)	25.0(54)[i]	47.7		0.949		600	0.2688
15	P				111		0.951		822	0.3441
16	S				223		0.952		1066	0.4155
17	Cl				410		0.953		1327	0.4851
18	Ar				711		0.955		1584	0.5558
19	K				1153		0.955		1828	0.6200
20	Ca				1732		0.956		2070	0.6732
21	Sc				2426		0.957		2375	0.7008
22	Ti				3226		0.957		2740	0.7360
23	V				4207		0.958		3151	0.7574
24	Cr				5130		0.958		3535	0.7690
25	Mn				6303		0.960		4435	0.7792
26	Fe				7850		0.960[j]		5130	0.7860

[a] Kernahan *et al.*, Ref. [57].
[b] Laughlin *et al.*, Ref. [40].
[c] This work.
[d] Buchet-Poulizac and Buchet, Ref. [37].
[e] Engström *et al.*, Ref. [27].
[f] Dumont *et al.*, Ref. [38].
[g] Kaystautas and Drouin, Ref. [39].
[h] Hardis *et al.*, Ref. [28].
[i] Grannow *et al.*, Ref. [29].
[j] Bhatia and Mason, Ref. [41].

For the s^2-sp transitions these are

$$<^1 S_0|r|^3P_1> = [\sin\theta_1]\mathcal{M}_{sp}$$
$$<^1 S_0|r|^1P_1> = [\cos\theta_1]\mathcal{M}_{sp}$$

and for sp-sd

$$<^3 P_0|r|^3D_1> = \left[\frac{1}{\sqrt{3}}\right]\mathcal{M}_{pd},$$
$$<^3 P'_1|r|^3D_1> = \left[\frac{1}{2}\cos\theta_1\right]\mathcal{M}_{pd},$$
$$<^3 P_2|r|^3D_1> = \left[\frac{1}{\sqrt{60}}\right]\mathcal{M}_{pd},$$
$$<^1 P'_1|r|^3D_1> = \left[\frac{1}{2}\sin\theta_1\right]\mathcal{M}_{pd},$$
$$<^3 P'_1|r|^3D'_2> = \left[\frac{\sqrt{3}}{2}\cos\theta_1\cos\theta_2 + \sin\theta_1\sin\theta_2\right]\mathcal{M}_{pd},$$
$$<^3 P_2|r|^3D'_2> = \left[\frac{1}{2}\cos\theta_2\right]\mathcal{M}_{pd},$$
$$<^1 P'_1|r|^3D'_2> = \left[\frac{\sqrt{3}}{2}\sin\theta_1\cos\theta_2 - \cos\theta_1\sin\theta_2\right]\mathcal{M}_{pd},$$
$$<^3 P_2|r|^3D_3> = \left[\sqrt{\frac{7}{5}}\right]\mathcal{M}_{pd},$$
$$<^3 P'_1|r|^1D'_2> = \left[\frac{\sqrt{3}}{2}\cos\theta_1\sin\theta_2 - \sin\theta_1\cos\theta_2\right]\mathcal{M}_{pd},$$
$$<^3 P_2|r|^1D'_2> = \left[\frac{1}{2}\sin\theta_2\right]\mathcal{M}_{pd},$$
$$<^1 P'_1|r|^1D'_2> = \left[\frac{\sqrt{3}}{2}\sin\theta_1\sin\theta_2 + \cos\theta_1\cos\theta_2\right]\mathcal{M}_{pd}.$$

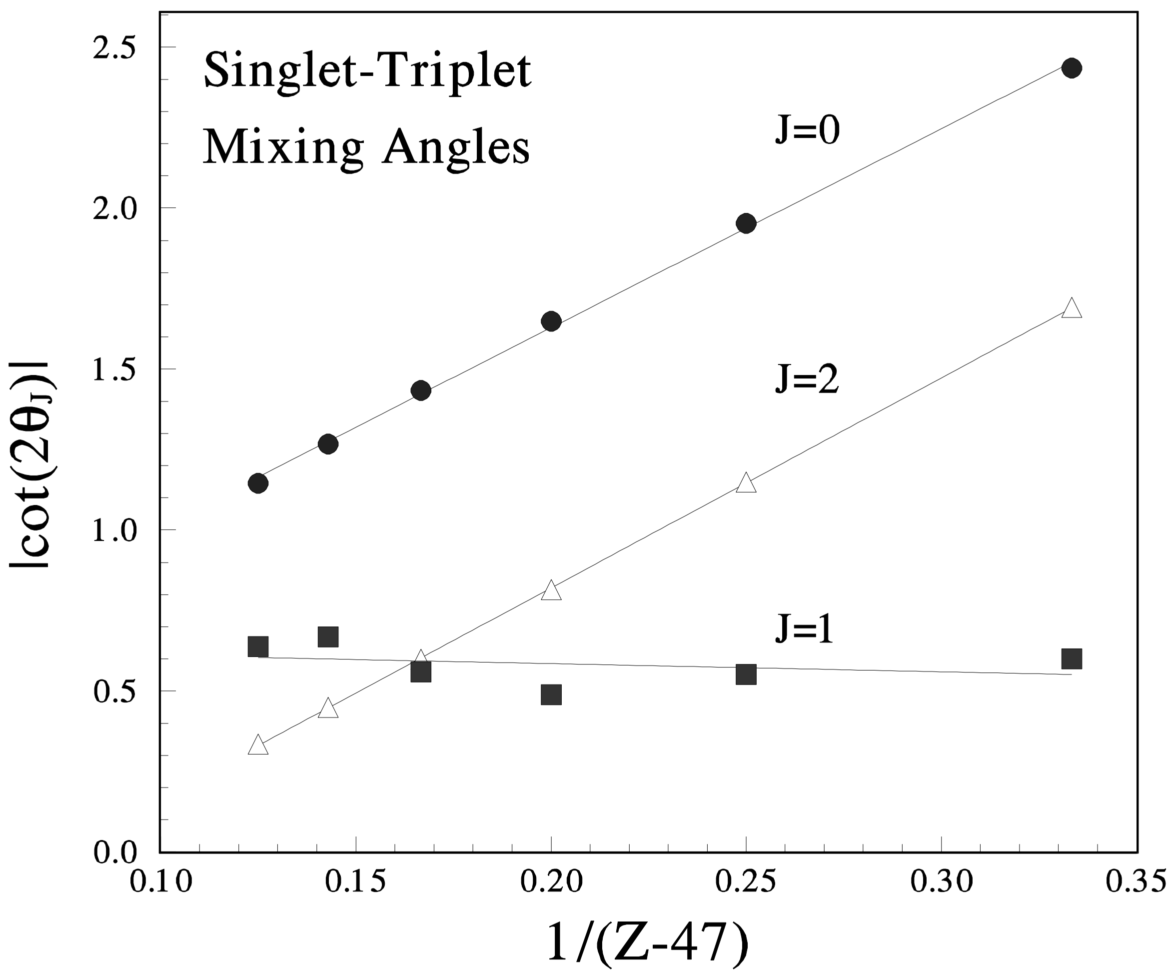

Singlet-Triplet
Mixing Angles
J=0
J=2
J=1
|cot(2θ_J)|
1/(Z-47)
0.0
0.5
1.0
1.5
2.0
2.5
0.10
0.15
0.20
0.25
0.30
0.35

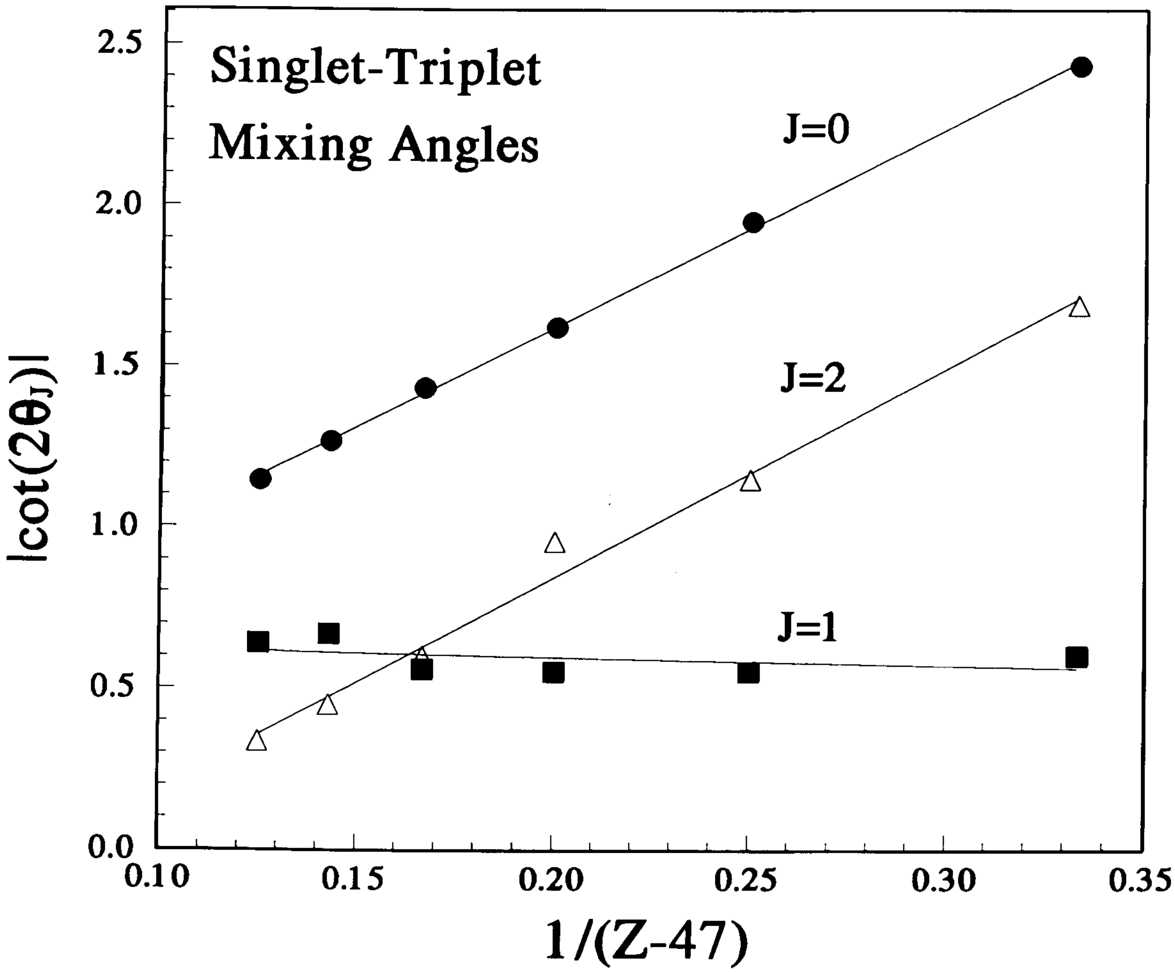
Singlet-Triplet
Mixing Angles
J=0
J=2
J=1
2.5
2.0
1.5
1.0
0.5
0.0
0.10
0.15
0.20
0.25
0.30
0.35
|cot(2θJ)|
1/(Z-47)

Table 4: Data base of experimental lifetime measurements (Exp) and semiempirical predictions (SE) based on this parametrization. Quoted measurement uncertainties are given in parentheses. The $^3P_1$ predictions are based on the $^1P_1$ measurements, and the $^3D_1$ and $^3D_3$ predictions are based on the $^3D_2$ measurements. A few recent calculations for the lifetimes of the $nsnp$ levels (Theo) are included for comparison.

	Ga II			In II			Tl II		
Level	Exp	Theo	SE[a]	Exp	Theo	SE[a]	Exp	Theo	SE[a]
$^3P_1$	-	2445[b]	2380	440(40)[c]	598[d]	449	39(3)[e]	36.3[f]	34.2
$^1P_1$	0.41(3)[g], 0.49(4)[h], 0.65(8)[i], 0.48(12)[j]		-	0.79(5)[k], 0.90(8)[l]		-	0.59(4)[e]	0.574[f]	-
$^3D_1$	-		0.66	0.86(3)[k]		0.86	-		-
$^3D_2$	0.67(6)[j]		-	0.91(3)[k]		-	-		-
$^3D_3$	-		0.69	0.94(3)[k]		1.00	-		-
$^1D_2$	0.67(4)[j], 0.73(7)[m]		-	0.77(3)[k]		-	5(1)[n], 7(1)[o]		-

[a] This work.
[b] Fleming and Hibbert [19].
[c] Peik *et al.* [22].
[d] Chou et al [20].
[e] Henderson and Curtis [23].
[f] Brage et al [21].
[g] Engström [24]
[h] Andersen *et al.* [25].
[i] Sørensen [26].
[j] Ansbacher *et al.* [27].
[k] Ansbacher *et al.* [28].
[l] Andersen *et al.* [29].
[m] Denne *et al.* [30].
[n] Andersen and Sørensen [31].
[o] Shimon and Erdevdi [32].

Table 2: Wavelengths (in air for $\lambda \geq 2000$ Å), multiplet fractions (in %), branching fractions (in %) and transition probability rates (in ns^{-1}) for the two supermultiplets. The transition probability rate predictions are based on the branching fractions obtained by this formalism and the measured and predicted lifetimes given in Table 3.

	Ga II				In II				Tl II			
Transition	λ(Å)	R_{ik}	BF	A_{ik}	λ(Å)	R_{ik}	BF	A_{ik}	λ(Å)	R_{ik}	BF	A_{ik}
$^1S_0$-$^3P_1$	2090.77	0.019	100	0.00042	2306.15	0.18	100	0.0023	1908.65	1.70	100	0.026
$^1S_0$-$^1P_1$	1414.40	99.98	100	2.19	1586.45	99.82	100	1.22	1321.70	98.30	100	1.69
$^3P_0$-$^3D_1$	1504.93	15.94	56.13	0.854	1672.00	16.57	57.17	0.665	1499.34	4.14	60.31	-
$^3P_1$-	1515.11	11.71	41.23	0.627	1702.57	11.70	40.38	0.470	1568.53	8.81	37.55	-
$^3P_2$-	1536.90	0.75	2.63	0.040	1777.57	0.69	2.38	0.028	1837.49	0.38	1.64	-
$^1P_1$-	2318.68	0.002	0.01	0.0001	2560.06	0.02	0.07	0.001	2469.18	0.12	0.50	-
SUM		28.40	100	1.522		28.98	100	1.163		23.45	100	-
$^3P_1$-$^3D_2$	1514.51	21.11	75.79	1.131	1700.08	21.20	77.22	0.849	1561.60	25.22	79.30	-
$^3P_2$-	1536.28	6.74	24.21	0.361	1774.86	6.23	22.70	0.249	1827.99	5.80	18.24	-
$^1P_1$-	2317.27	0.002	0.01	$<10^{-4}$	2554.44	0.023	0.08	0.001	2452.04	0.78	2.46	-
SUM		27.85	100	1.493		27.46	100	1.099		31.80	100	-
$^3P_2$-$^3D_3$	1535.31	27.03	100	1.448	1770.66	25.11	100	1.063	1814.85	33.49	100	-
$^3P_1$-$^1D_2$	1275.94	0.16	0.02	0.0003	1417.81	0.20	1.08	0.014	1593.19	3.21	28.52	0.048
$^3P_2$-	1291.36	$<10^{-3}$	$<10^{-3}$	10^{-5}	1469.44	0.002	0.01	0.0001	1871.43	0.05	0.44	0.001
$^1P_1$-	1802.25	16.70	99.98	1.460	1966.71	18.25	98.91	1.285	2530.88	7.99	71.04	0.118
SUM		16.72	100	1.460		18.45	100	1.299		11.25	100	0.167

TABLE III. Comparison of predicted transition probabilities and branching fractions for the 5s5p ^{3}P - 5s5d ^{3}D manifold in In II.

	$A_{ik}(ns^{-1})$			BF(%)		
Transition	RQDO[a]	RQDO[b]	SE[c]	RQDO[a]	RQDO[b]	SE[c]
5s5p $^3P_0$ - 5s5d $^3D_1$	0.696	0.593	0.665	57.9	57.9	57.17
5s5p $^3P_1$ -	0.483	0.412	0.470	40.2	40.2	40.38
5s5p $^3P_2$ -	0.023	0.020	0.028	1.9	1.9	2.38
5s5p $^1P_1$ -	-	-	0.001	-	-	0.07
5s5p $^3P_1$ - 5s5d $^3D_2$	0.873	0.747	0.849	80.1	80.1	77.22
5s5p $^3P_2$ -	0.218	0.186	0.249	19.9	19.9	22.70
5s5p $^1P_1$ -	-	-	0.001	-	-	0.08
5s5p $^3P_2$ - 5s5d $^3D_3$	0.878	0.754	1.063	100.	100.	100.

[a] Lavín and Martin, rel. quantum defect orbital [15].

[b] Lavín and Martin, rel. quantum defect orbital with polarization [15].

[c] This work.

Example where transitions connect these two types of IC configurations

Pb Sequence

gs $5d^{10}6s^2 6p^2$

1st ex. $5d^{10}6s^2 6p7s$

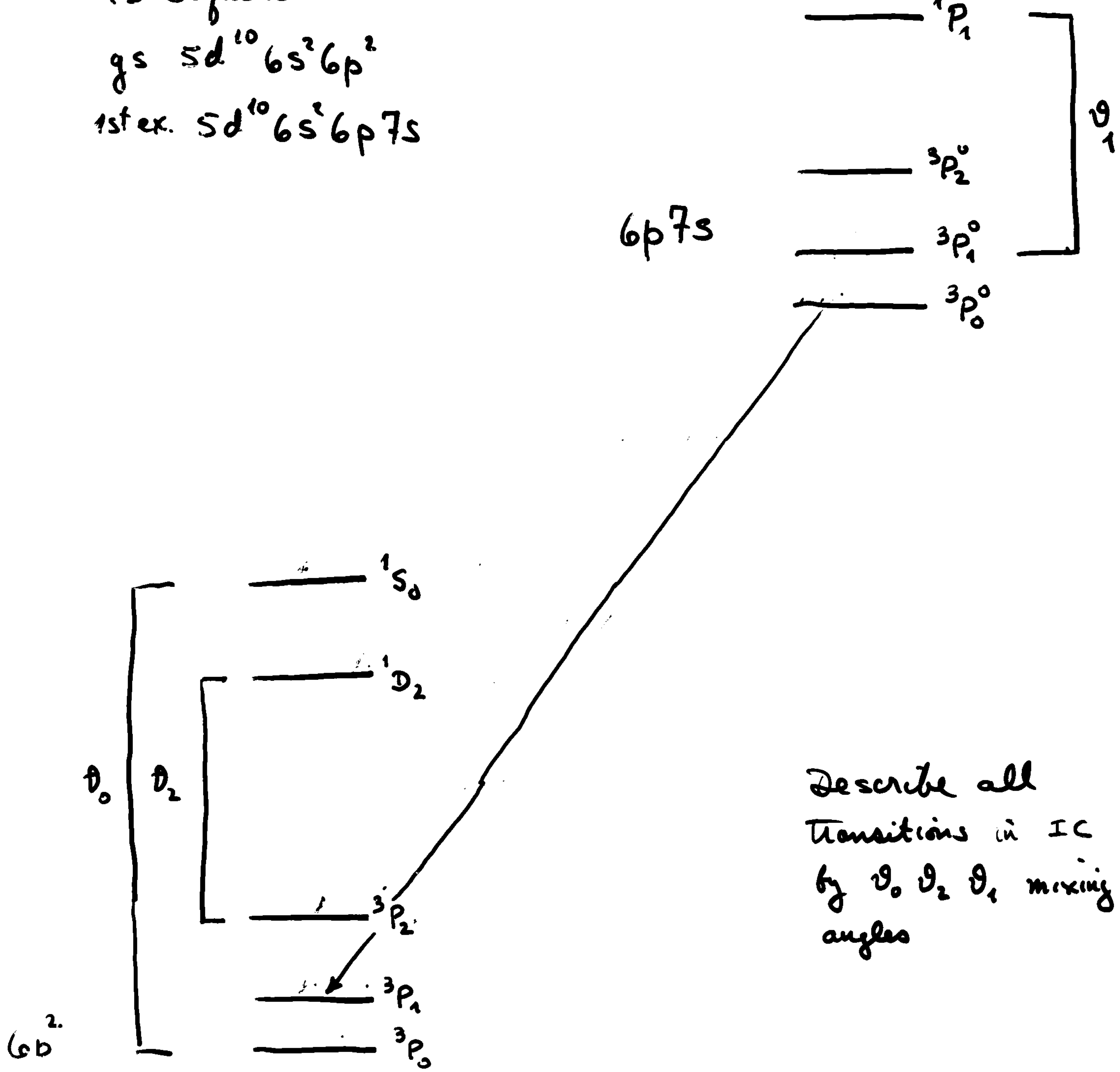

Describe all transitions in IC by ϑ_0 ϑ_2 ϑ_1 mixing angles

np^2

	$^3P_0$	$^3P_1$	$^3P_2$	$^1D_2$	$^1S_0$
$^3P_0$	$E_0-5F_2-\zeta_1$	0	0	0	$-\sqrt{2}\,\zeta_0$
$^3P_1$	0	$E_0-5F_2-\zeta_1/2$	0	0	0
$^3P_2$	0	0	$E_0-5F_2+\zeta_1/2$	$\zeta_2/\sqrt{2}$	0
$^1D_2$	0	0	$\zeta_2/\sqrt{2}$	F_0+F_2	0
$^1S_0$	$-\sqrt{2}\,\zeta_0$	0	0	0	F_0+10F_2

This is diagonalizid by the transformation $J^{-1}\mathcal{H}J$, where

$$J = \begin{bmatrix} \cos\vartheta_0 & 0 & 0 & 0 & \sin\vartheta_0 \\ 0 & 1 & \cos\vartheta_1 & \sin\vartheta_1 & 0 \\ 0 & 0 & -\sin\vartheta_1 & \cos\vartheta_1 & 0 \\ -\sin\vartheta_0 & 0 & 0 & 0 & \cos\vartheta_0 \end{bmatrix}$$

with the energy levels

$$^3P_0' = E_0 + 5F_2/2 - \zeta_1/2 - \Delta_0$$

$$^3P_1 = E_0 - 5F_2 - \zeta_1/2$$

$$^3P_2' = E_0 - 2F_2 + \zeta_1/4 - \Delta_2$$

$$^1D_2' = E_0 - 2F_2 + \zeta_1/4 + \Delta_2$$

$$^1S_0' = E_0 + 5F_2/2 - \zeta_1/2 + \Delta_2$$

$$\begin{cases} \Delta_0 = \sqrt{(15F_2/2 + \zeta_1/2)^2 + 2\zeta_0^2} \\ \Delta_2 = \sqrt{(3F_2 - \zeta_1/4)^2 + \zeta_2^2/2} \end{cases}$$

where the angles are

$$\cot 2\vartheta_0 = \frac{15F_2 + \zeta_1}{\sqrt{8}\,\zeta_0}$$

$$\cot 2\vartheta_2 = \frac{12F_2 - \zeta_1}{\sqrt{8}\,\zeta_2}$$

levels of the ground configuration p^2 can be deduced from this formalism using the LS coupling angular transition matrices [12, 13]. The nonvanishing values are

$$\langle {}^3P_0^o|r|{}^3P_1\rangle = \langle {}^1P_1^o|r|{}^1S_0\rangle = -\langle {}^3P_1^o|r|{}^3P_0\rangle = -\sqrt{20} \tag{10}$$

$$2\langle {}^3P_2^o|r|{}^3P_1\rangle = -2\langle {}^3P_1^o|r|{}^3P_2\rangle = \langle {}^1P_1^o|r|{}^1D_2\rangle = 10 \tag{11}$$

$$\sqrt{5}\langle {}^3P_1^o|r|{}^3P_1\rangle = \langle {}^3P_2^o|r|{}^3P_2\rangle = \sqrt{75}. \tag{12}$$

These equations yield, for the upper level ${}^3P_1^{o\prime}$

$$\langle {}^3P_0{}'|\mathbf{r}|{}^3P_1^{o\prime}\rangle = -\sqrt{20}\cos(\theta_1+\theta_0)\ \langle p^2|r|sp\rangle \tag{13}$$

$$\langle {}^3P_1{}'|\mathbf{r}|{}^3P_1^{o\prime}\rangle = \sqrt{15}\cos\theta_1\ \langle \mathrm{p}^2|r|\mathrm{sp}\rangle \tag{14}$$

$$\langle {}^3P_2{}'|\mathbf{r}|{}^3P_1^{o\prime}\rangle = 5(2\sin\theta_1\sin\theta_2+\cos\theta_1\cos\theta_2)\ \langle \mathrm{p}^2|r|\mathrm{sp}\rangle \tag{15}$$

$$\langle {}^1D_2{}'|\mathbf{r}|{}^3P_1^{o\prime}\rangle = -5(2\sin\theta_1\cos\theta_2-\cos\theta_1\sin\theta_2)\ \langle \mathrm{p}^2|r|\mathrm{sp}\rangle \tag{16}$$

$$\langle {}^1S_0{}'|\mathbf{r}|{}^3P_1^{o\prime}\rangle = -\sqrt{20}\sin(\theta_1+\theta_0)\ \langle \mathrm{p}^2|r|\mathrm{sp}\rangle, \tag{17}$$

for the upper level ${}^3P_2^{o\prime}$

$$\langle {}^3P_1{}'|\mathbf{r}|{}^3P_2^{o\prime}\rangle = 5\ \langle \mathrm{p}^2|r|\mathrm{sp}\rangle \tag{18}$$

$$\langle {}^3P_2{}'|\mathbf{r}|{}^3P_2^{o\prime}\rangle = \sqrt{15}\cos\theta_2\ \langle \mathrm{p}^2|r|\mathrm{sp}\rangle \tag{19}$$

$$\langle {}^1D_2{}'|\mathbf{r}|{}^3P_2^{o\prime}\rangle = \sqrt{15}\sin\theta_2\ \langle \mathrm{p}^2|r|\mathrm{sp}\rangle, \tag{20}$$

and for the upper level ${}^1P_1^{o\prime}$

$$\langle {}^3P_0{}'|\mathbf{r}|{}^1P_1^{o\prime}\rangle = -\sqrt{20}\sin(\theta_1+\theta_0)\ \langle \mathrm{p}^2|r|\mathrm{sp}\rangle \tag{21}$$

$$\langle {}^3P_1{}'|\mathbf{r}|{}^1P_1^{o\prime}\rangle = \sqrt{15}\sin\theta_1\ \langle \mathrm{p}^2|r|\mathrm{sp}\rangle \tag{22}$$

$$\langle {}^3P_2{}'|\mathbf{r}|{}^1P_1^{o\prime}\rangle = 5(2\cos\theta_1\sin\theta_2-\sin\theta_1\cos\theta_2)\ \langle \mathrm{p}^2|r|\mathrm{sp}\rangle \tag{23}$$

$$\langle {}^1D_2{}'|\mathbf{r}|{}^1P_1^{o\prime}\rangle = -5(2\cos\theta_1\cos\theta_2+\sin\theta_1\sin\theta_2)\ \langle \mathrm{p}^2|r|\mathrm{sp}\rangle \tag{24}$$

$$\langle {}^1S_0{}'|\mathbf{r}|{}^1P_1^{o\prime}\rangle = -\sqrt{20}\cos(\theta_1+\theta_0)\ \langle \mathrm{p}^2|r|\mathrm{sp}\rangle. \tag{25}$$

It should be noted that in a fully relativistic Dirac treatment the corresponding expressions will involve two separate jj coupled radial transition matrices, and reduce to equations (13-25) only if these two radial matrices are equal. Theoretical studies of these relativistic corrections have been presented elsewhere [14].

For pure sp and p^2 configurations the energy levels (and thereby the mixing angles) are specified [10] by three parameters (F_0, G_1, ζ_p for sp and F_0, F_2, ζ_{pp} for p^2, in the notation of Ref.[13]). Since the sp and p^2 configurations contain four and five levels respectively, the specification of these three parameters is overdetermined. Here this was treated by using the average energies ε_J of the J=0,1,2 levels to make an exactly determined parametrization, computing the singlet-triplet splittings from this parametrization, and then using the deviations as a measure of the validity of the

Table 1. Comparison of semiempirical and measured branching fractions (in %) for Si I and Ge I. SE denotes the semiempirical estimates of [3]. Expt denotes experimental measurements as cited, with parentheses indicating quoted uncertainties in the last figure.

	Si I			Ge I		
Transition	SE	Expt [6]	Expt [7]	SE	Expt [8]	Expt [9]
$^3P'_0 \leftarrow {}^3P^{o\prime}_1$	33.3	33.3(17)	33.3(3)	31.2	32.5(16)	32.9
$^3P_1 \leftarrow$	24.7	24.7(13)	24.7(4)	21.2	22.1(11)	20.3
$^3P'_2 \leftarrow$	41.1	40.6(21)	40.7(4)	38.3	37.1(19)	36.1
$^1D'_2 \leftarrow$	0.88	1.20(11)	1.2(1)	8.8	8.1(8)	10.3
$^1S'_0 \leftarrow$	0.06	<0.20(6)	<0.20(6)	0.52	0.23(2)	0.38
$^3P_1 \leftarrow {}^3P^o_2$	25.2	24.6(13)	24.6(3)	26.4	27.2(14)	31.0
$^3P'_2 \leftarrow$	74.8	75.4(36)	75.4(3)	73.1	72.1(14)	67.8
$^1D'_2 \leftarrow$	0.020	0.027(4)	0.027(4)	0.53	0.72(7)	1.3
$^3P'_0 \leftarrow {}^1P^{o\prime}_1$	0.24	0.34(3)	0.30(2)	2.9	4.6(5)	4.5
$^3P_1 \leftarrow$	0.25	0.27(3)	0.20(2)	3.3	3.6(4)	3.6
$^3P'_2 \leftarrow$	0.15	0.25(3)	0.20(2)	1.0	1.68(17)	1.7
$^1D'_2 \leftarrow$	92.0	93.4(47)	93.4(2)	86.2	86.1(14)	83.2
$^1S'_0 \leftarrow$	7.4	5.7(3)	5.70(12)	6.6	4.0(4)	7.0

Table 4. Transition wavelengths and semiempirical branching fractions (BF, in %) for ions in the Si sequence.

Transition	P II λ (Å)	P II BF	S III λ (Å)	S III BF	Cl IV λ (Å)	Cl IV BF	Ar V λ (Å)	Ar V BF
$^3P'_0 \leftarrow {}^3P^{o\prime}_1$	1115.82	33.1	681.49	32.8	464.28	32.4	337.58	31.9
$^3P_1 \leftarrow$	1155.01	24.5	682.88	24.2	465.34	23.8	338.45	23.2
$^3P'_2 \leftarrow$	1158.82	41.0	685.38	40.8	467.19	40.7	339.91	40.5
$^1D'_2 \leftarrow$	1284.33	1.3	784.47	1.9	495.98	2.7	357.24	3.8
$^1S'_0 \leftarrow$	1534.49	0.12	836.28	0.22	546.92	0.32	387.12	0.49
$^3P_1 \leftarrow {}^3P^o_2$	1149.96	25.2	680.97	25.2	463.01	25.2	336.57	25.3
$^3P'_2 \leftarrow$	1153.73	74.8	683.46	74.7	464.84	74.6	338.01	74.4
$^1D'_2 \leftarrow$	1278.08	$<10^{-3}$	736.25	0.11	493.34	0.21	355.14	0.37
$^3P'_0 \leftarrow {}^1P^{o\prime}_1$	1124.95	0.22	673.86	0.27	455.68	0.34	331.91	0.47
$^3P_1 \leftarrow$	1127.04	0.25	675.22	0.34	456.70	0.46	332.75	0.65
$^3P'_2 \leftarrow$	1130.66	0.11	677.66	$<10^{-3}$	458.48	$<10^{-3}$	334.16	$<10^{-3}$
$^1D'_2 \leftarrow$	1249.83	88.8	729.52	87.2	486.18	86.1	350.89	85.2
$^1S'_0 \leftarrow$	1485.50	10.6	824.82	12.1	535.03	13.0	379.68	13.6

Table 5. Transition wavelengths and semiempirical branching fractions (in %) for ions in the Ge sequence.

	As II		Se III		Br IV	
Transition	λ (Å)	BF	λ (Å)	BF	λ (Å)	BF
$^3P'_0 \leftarrow {}^3P^{o\prime}_1$	1263.77	29.8	788.76	28.1	549.93	28.8
$^3P_1 \leftarrow$	1280.99	20.0	799.74	18.4	557.98	18.6
$^3P'_2 \leftarrow$	1305.70	38.7	814.04	38.6	567.45	40.8
$^1D'_2 \leftarrow$	1448.59	10.5	879.13	13.4	603.68	10.5
$^1S'_0 \leftarrow$	1768.98	0.99	1017.30	1.5	676.48	1.3
$^3P_1 \leftarrow {}^3P^o_2$	1243.08	26.2	777.30	26.1	545.44	26.1
$^3P'_2 \leftarrow$	1266.34	72.7	790.80	72.0	554.48	70.8
$^1D'_2 \leftarrow$	1400.30	1.1	852.09	1.87	589.03	3.1
$^3P'_0 \leftarrow {}^1P^{o\prime}_1$	1207.45	2.34	759.56	2.70	534.47	1.9
$^3P_1 \leftarrow$	1223.16	2.95	769.74	3.50	542.07	3.0
$^3P'_2 \leftarrow$	1245.67	0.41	782.97	0.32	551.00	$<10^{-5}$
$^1D'_2 \leftarrow$	1375.07	84.4	843.00	82.2	585.08	82.6
$^1S'_0 \leftarrow$	1660.56	9.90	968.24	11.3	663.23	12.6

Table III. *Wavelengths and semiempirical, theoretical and experimental branching fractions for $5s^2 5p^2$–$5s^2 5p6s$ transitions in Sn I and Sb II.*

	Sn I						Sb II		
		BF(%)						BF(%)	
Transition	λ(Å)[a]	SE[b]	B[c]	L[d]	CB[e]	M[f]	λ(Å)[a]	SE[b]	B[c]
${}^3P'_0 \leftarrow {}^3P^{o\prime}_1$	2863.32	32.3	28.9	27	37	40	1438.11	30.2	38.4
${}^3P'_1 \leftarrow$	3009.13	17.5	20.9	17	27	28	1504.19	16.1	23.8
${}^3P'_2 \leftarrow$	3175.03	39.7	41.8	39	22	22	1565.50	43.4	31.9
${}^1D'_2 \leftarrow$	3801.01	10.0	8.2	17	14	11	1762.24	9.5	5.7
${}^1S'_0 \leftarrow$	5631.71	0.5	0.2	-	0.3	0.2	2190.85	0.8	0.2
${}^3P'_1 \leftarrow {}^3P^o_2$	2706.50	28.3	25.3	22	30	32	1384.66	27.8	14.8
${}^3P'_2 \leftarrow$	2839.98	68.5	72.1	71	64	63	1436.45	65.5	48.4
${}^1D'_2 \leftarrow$	3330.61	3.2	2.6	7	6	5	1600.39	6.6	36.8
${}^3P'_0 \leftarrow {}^1P^{o\prime}_1$	2546.55	4.2	3.6	8	21	25	1317.54	3.0	1.6
${}^3P'_1 \leftarrow$	2661.24	6.8	3.6	4	13	14	1372.79	6.0	1.8
${}^3P'_2 \leftarrow$	2790.18	0.01	0.8	-	-	-	1423.68	0.6	0.5
${}^1D'_2 \leftarrow$	3262.33	82.2	84.3	88	60	57	1584.56	80.2	84.7
${}^1S'_0 \leftarrow$	4624.75	6.8	7.7	-	6	4	1923.32	10.2	11.5

[a] Air wavelengths for $\lambda > 2000$ Å.
[b] Semiempirical, this work.
[c] Bieroń *et al.* [18], theoretical (MCDM-EAL with Babushkin gauge).
[d] Lotrian *et al.* [19], arc emission.
[e] Corliss and Bozman [20], arc emission.
[f] Meggers *et al.* [21], arc emission.

Table IV. *Wavelengths and semiempirical branching fractions for $5s^2 5p^2$-$5s^2 5p6s$ transitions in multiply charged ions of the Sn sequence.*

	Te III		I IV		Xe V		Cs VI	
Transition	λ(Å)	BF(%)	λ(Å)	BF(%)	λ(Å)	BF(%)	λ(Å)	BF(%)
${}^3P'_0 \leftarrow {}^3P^{o\prime}_1$	928.30	30.1	666.29	30.0	512.82	31.1	410.31	31.0
${}^3P'_1 \leftarrow$	971.19	15.6	698.04	15.3	538.56	16.1	431.89	15.6
${}^3P'_2 \leftarrow$	1004.45	45.1	718.89	49.0	552.94	50.0	442.30	51.2
${}^1D'_2 \leftarrow$	1106.63	8.5	783.98	5.0	600.38	2.4	479.25	1.8
${}^1S'_0 \leftarrow$	1310.56	0.7	885.67	0.7	664.81	0.4	522.72	0.3
${}^3P'_1 \leftarrow {}^3P^o_2$	913.59	27.6	649.31	27.6	500.55	27.6	401.97	27.7
${}^3P'_2 \leftarrow$	942.97	63.6	667.31	57.8	512.95	54.3	410.98	51.1
${}^1D'_2 \leftarrow$	1032.46	8.9	723.04	14.6	553.53	18.1	442.09	21.2
${}^3P'_0 \leftarrow {}^1P^{o\prime}_1$	866.40	2.1	619.65	1.5	469.19	0.7	378.46	0.6
${}^3P'_1 \leftarrow$	903.64	5.6	647.02	5.2	490.64	4.3	396.75	4.4
${}^3P'_2 \leftarrow$	932.37	1.4	664.89	5.2	502.55	9.4	405.52	11.9
${}^1D'_2 \leftarrow$	1019.77	79.2	720.20	74.8	541.43	71.6	436.37	68.6
${}^1S'_0 \leftarrow$	1190.47	11.7	805.12	13.3	593.28	14.1	472.11	14.6

S II

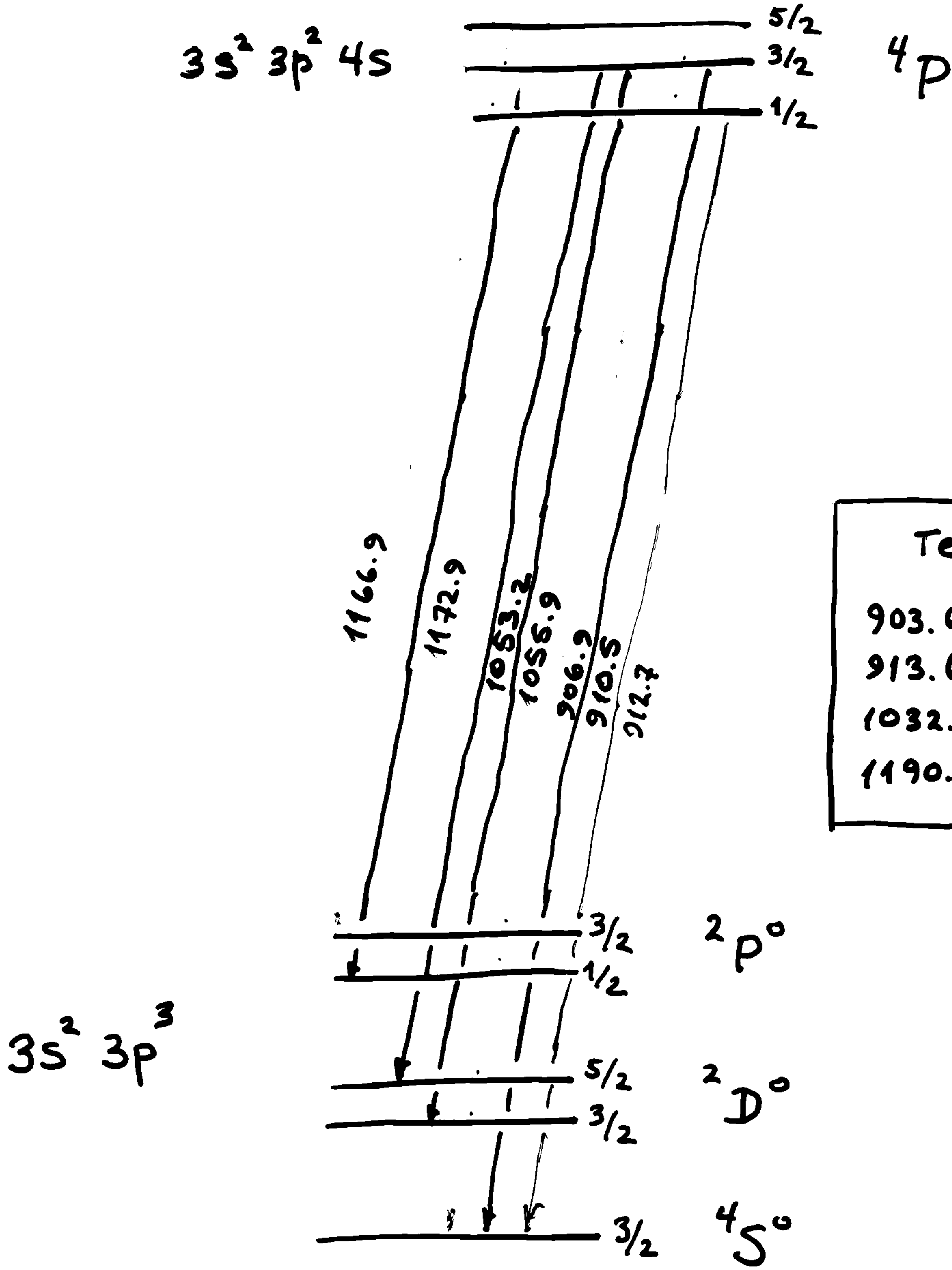

Te III	
903.6	5.6%
913.6	27.6%
1032.5	8.9%
1190.5	11.7%

Dirac Formulation

$$< \, ^3P_1 \, |\mathbf{r}| \, ^3P_0^o >= \sqrt{20} R_{31} \tag{1}$$

$$< \, ^3P_0 \, |\mathbf{r}| \, ^3P_1^o >= -\tfrac{\sqrt{20}}{3}[(R_{31} + 2R_{11}) \cos\theta_0 \cos\theta_1 - (2R_{31} + R_{11}) \sin\theta_0 \sin\theta_1 + \sqrt{2}(R_{31} - R_{11}) \sin(\theta_0 - \theta_1)] \tag{2}$$

$$< \, ^3P_1 \, |\mathbf{r}| \, ^3P_1^o >= \tfrac{\sqrt{15}}{3} \left[(2R_{31} + R_{11}) \cos\theta_1 + \sqrt{2}(R_{31} - R_{11}) \sin\theta_1\right] \tag{3}$$

$$< \, ^3P_2 \, |\mathbf{r}| \, ^3P_1^o >= \tfrac{5}{3}[(4R_{31} + 2R_{11}) \sin\theta_1 \sin\theta_2 + (4R_{31} - R_{11}) \cos\theta_1 \cos\theta_2 - \sqrt{2}(R_{31} - R_{11}) \sin(\theta_1 - \theta_2)] \tag{4}$$

$$< \, ^1D_2 \, |\mathbf{r}| \, ^3P_1^o >= -\tfrac{5}{3}[(4R_{31} + 2R_{11}) \sin\theta_1 \cos\theta_2 - (4R_{31} - R_{11}) \cos\theta_1 \sin\theta_2 + \sqrt{2}(R_{31} - R_{11}) \cos(\theta_1 - \theta_2)] \tag{5}$$

$$< \, ^1S_0 \, |\mathbf{r}| \, ^3P_1^o >= -\tfrac{\sqrt{20}}{3}[(R_{31} + 2R_{11}) \sin\theta_0 \cos\theta_1 + (2R_{31} + R_{11}) \cos\theta_0 \sin\theta_1 - \sqrt{2}(R_{31} - R_{11}) \cos(\theta_0 - \theta_1)] \tag{6}$$

Intermediate Coupling Specification of Branching Fractions

Bi II $6s^26p^2 - 6s^26p7s$

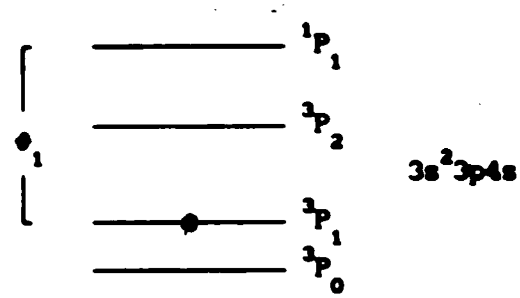

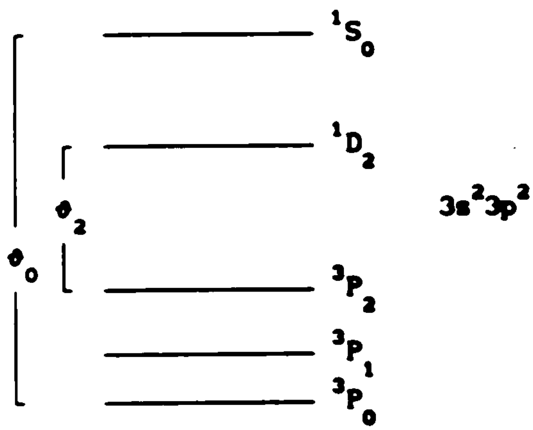

$$< {}^3P_0\ |\mathbf{r}|\ {}^3P_1^o > = -\sqrt{20}\cos(\theta_1 + \theta_0) < p^2|r|sp >$$

$$< {}^3P_1\ |\mathbf{r}|\ {}^3P_1^o > = \sqrt{15}\cos\theta_1 < p^2|r|sp >$$

$$< {}^3P_2\ |\mathbf{r}|\ {}^3P_1^o > = 5(2\sin\theta_1\sin\theta_2 + \cos\theta_1\cos\theta_2) < p^2|r|sp >$$

$$< {}^1D_2\ |\mathbf{r}|\ {}^3P_1^o > = -5(2\sin\theta_1\cos\theta_2 - \cos\theta_1\sin\theta_2) < p^2|r|sp >$$

$$< {}^1S_0\ |\mathbf{r}|\ {}^3P_1^o > = -\sqrt{20}\sin(\theta_1 + \theta_0) < p^2|r|sp > .$$

Table 2: Pb I branching fractions and transition probability rates for the $^3P_1^o$ upper level in the $6s^26p^2$-$6s^26p7s$ multiplet.

Transition	λ(Å)[a]	BF(N)[b]	BF(R)[c]	BF(M)[d]	$A(ns^{-1})$[e]
$^3P_0$ - $^3P_1^o$	2833.89	0.489	0.310	0.324	0.0529
$^3P_1$ -	3640.61	0.128	0.166	0.188	0.0284
$^3P_2$ -	4058.95	0.381	0.520	0.500	0.0889
$^1D_2$ -	7230.96	0.0029	0.0040	0.0005	0.00068
$^1S_0$ -	17181	$7\text{x}10^{-5}$	$3\text{x}10^{-5}$	-	$6\text{x}10^{-6}$

[a] Vacuum wavelengths.
[b] Nonrelativistic, R_{13}/R_{11}=1.
[c] Relativistic, R_{13}/R_{11}=1.4590.
[d] Measured, Ref.[22].
[e] Relativistic, using BF(R) and τ=5.84 ns.

Table 3: Bi II branching fractions and transition probability rates for the $^3P_1^o$ upper level in the $6s^26p^2$-$6s^26p7s$ multiplet.

Transition	λ(Å)[a]	BF(N)[b]	BF(R)[c]	$A(ns^{-1})$[d]
$^3P_0$ - $^3P_1^o$	1436.83[e]	0.43	0.25	0.20
$^3P_1$ -	1777.11[e]	0.12	0.16	0.13
$^3P_2$ -	1902.31[f]	0.44	0.59	0.47
$^1D_2$ -	2804.2[e]	0.004	0.005	0.004
$^1S_0$ -	3933.3[e]	0.0002	0.0009	0.0002

[a] Vacuum wavelengths.
[b] Nonrelativistic, R_{13}/R_{11}=1.
[c] Relativistic, R_{13}/R_{11}=1.4224.
[d] Relativistic, using BF(R) and τ=1.56 ns.
[e] Reader and Corliss, Ref.[26].
[f] Wahlgren *et al.*, Ref.[27].

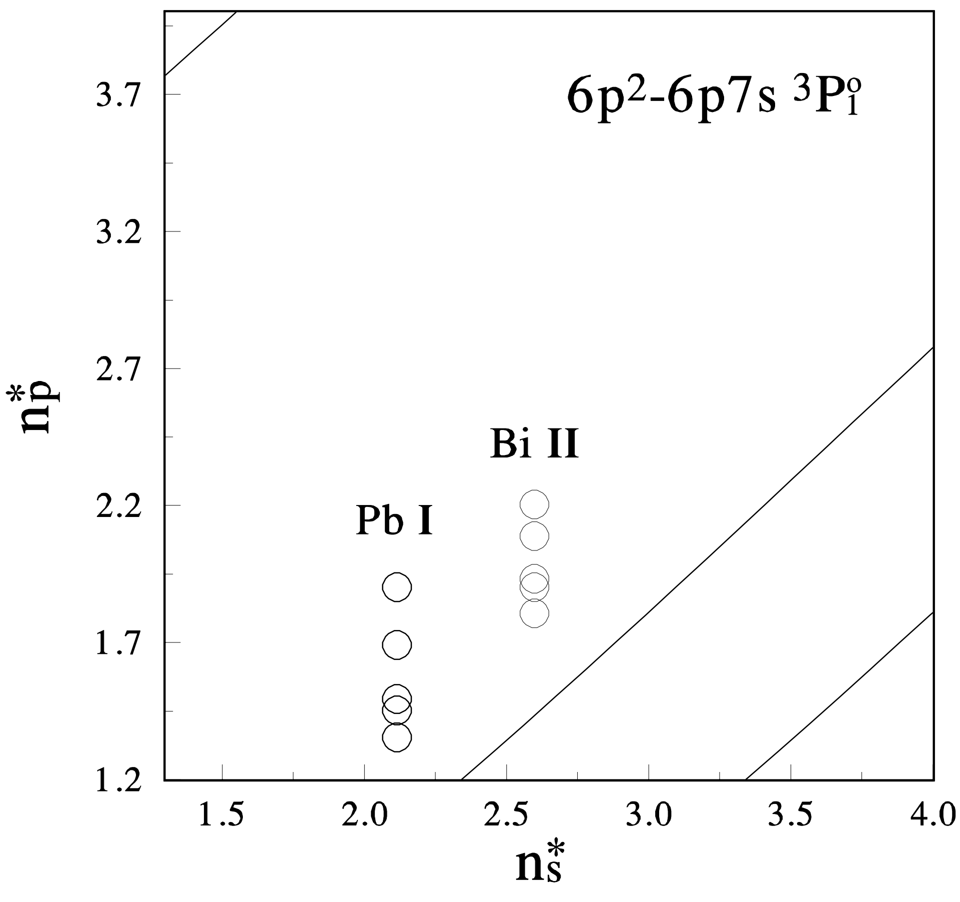

$6p^2$-$6p7s\ ^3P^o_1$
Bi II
Pb I
3.7
3.2
2.7
2.2
1.7
1.2
1.5
2.0
2.5
3.0
3.5
4.0
n^*_p
n^*_s

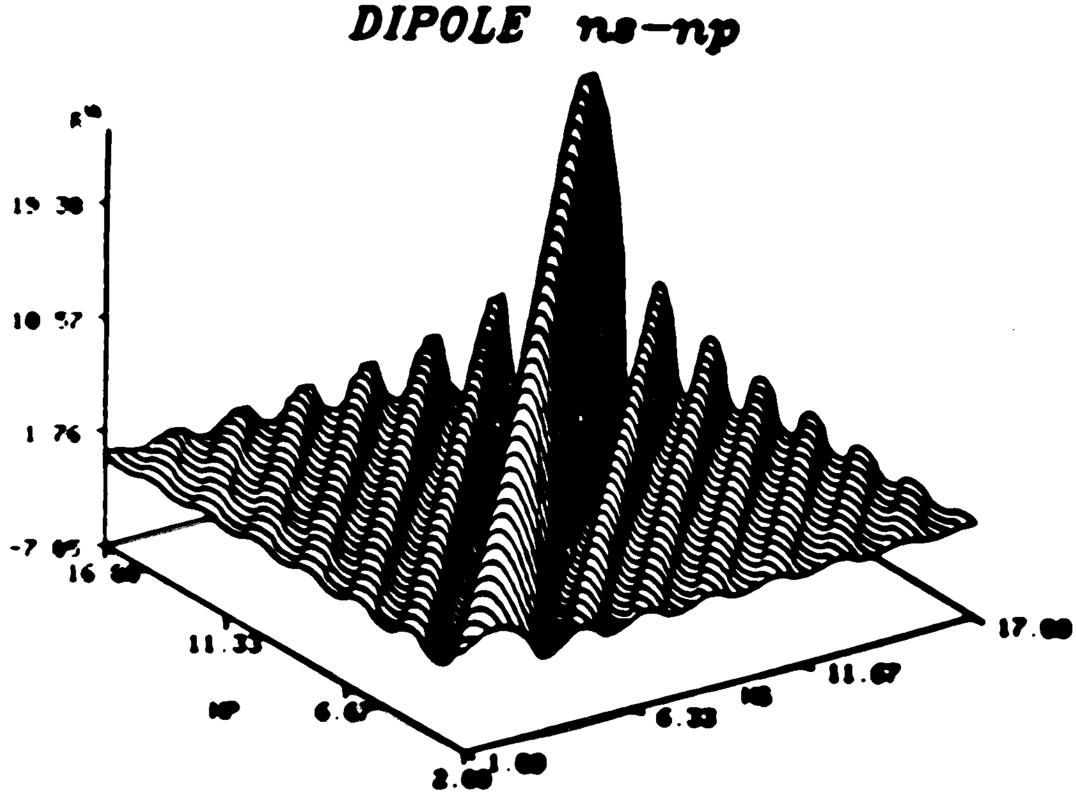
DIPOLE ns−np
19.38
10.57
1.76
16.00
11.33
NP
6.67
2.00
1.00
6.33
NS
11.67
17.00

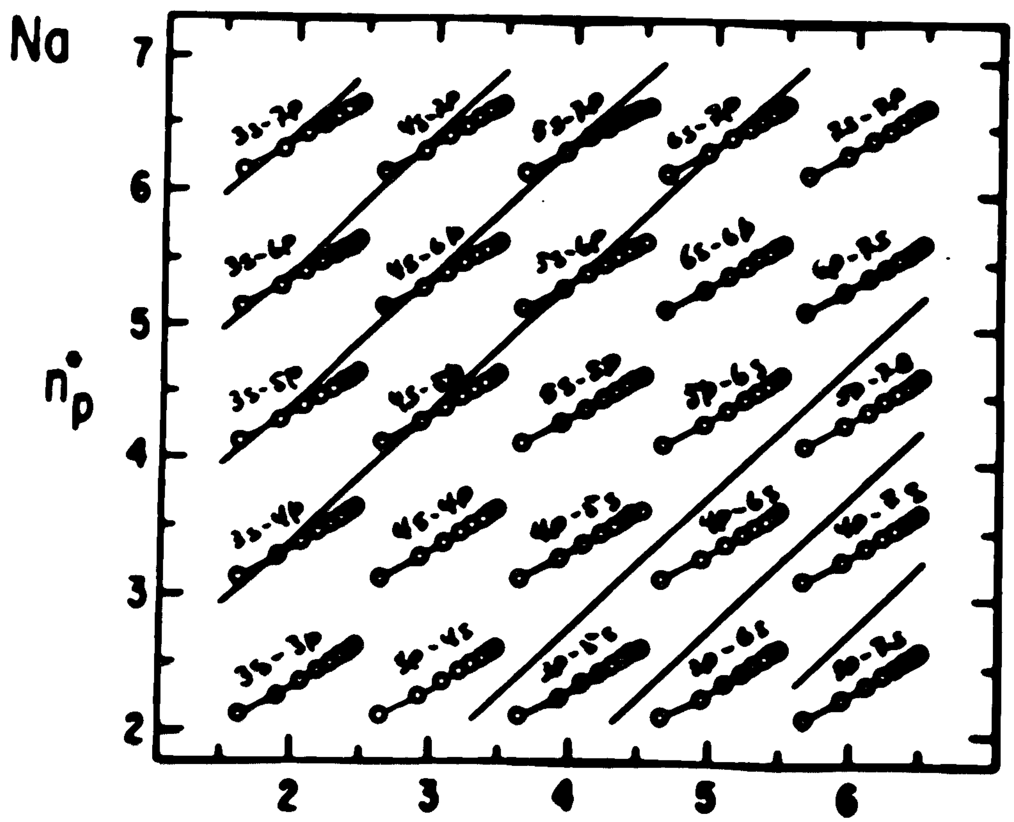
Na
7
6
5
4
3
2
n_p^*
2
3
4
5
6
n_s^*

DIPOLE ns–np

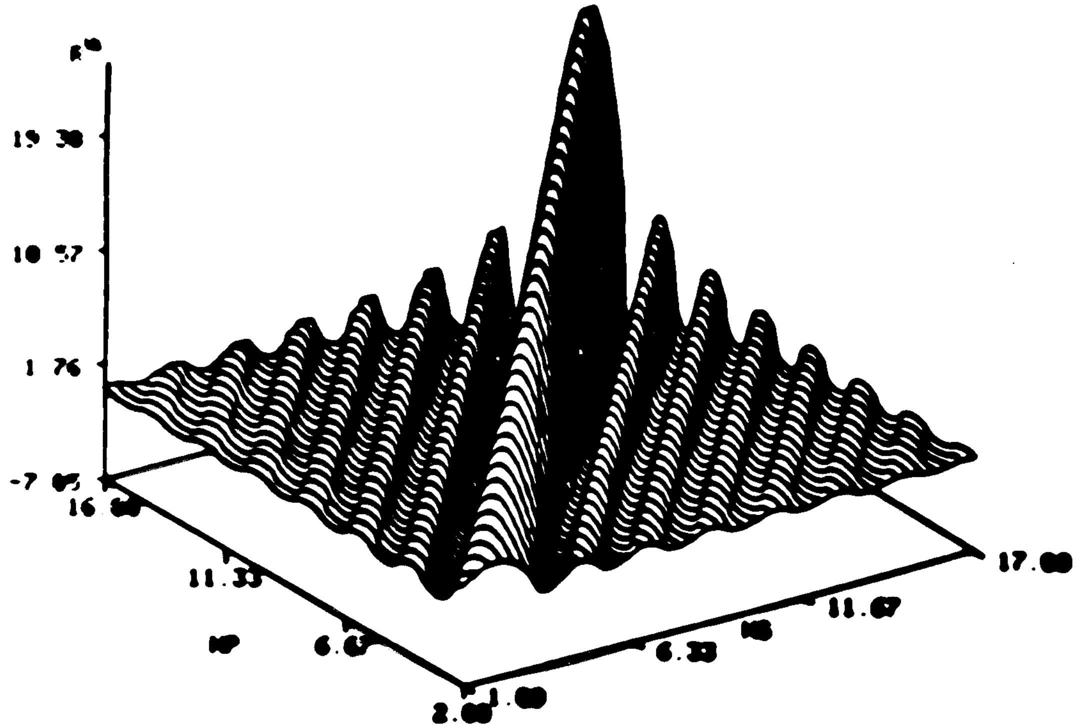

19.38
10.57
1.76
-7.05
16.00
11.33
NP
17.00
11.67
NS
6.33
1.00
2.00

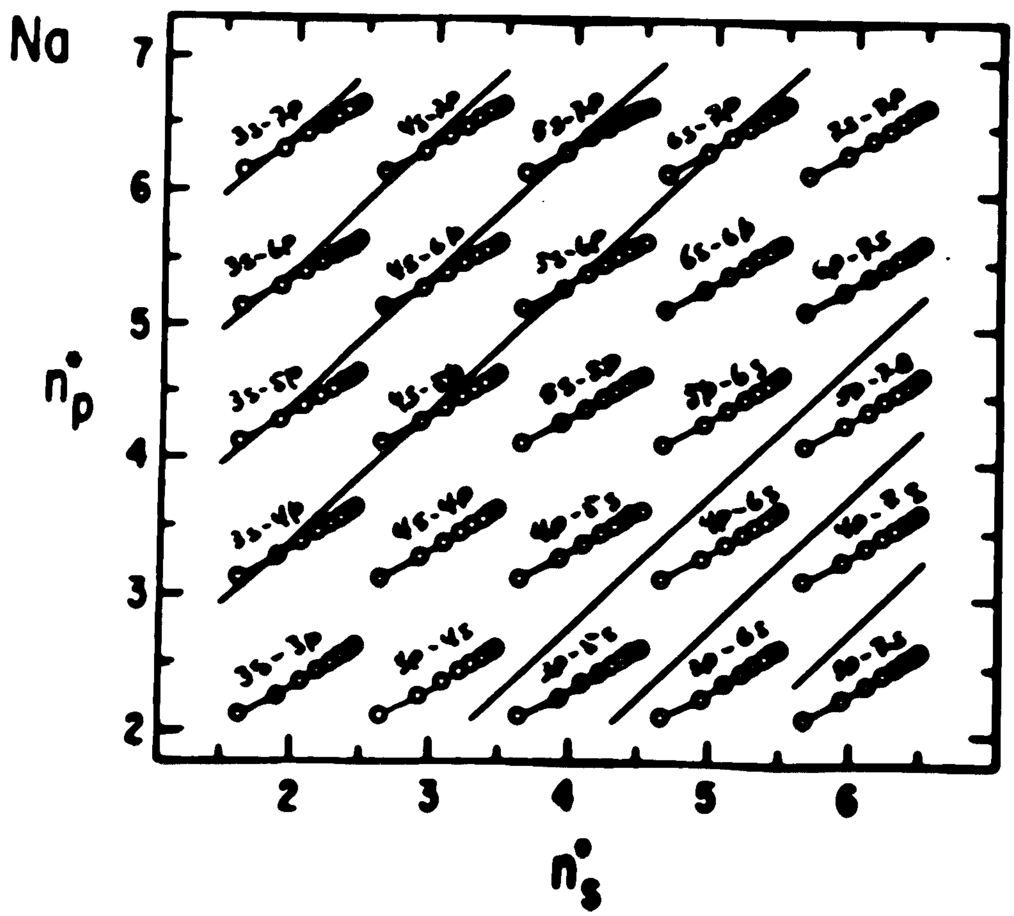

Na
7
6
5
4
3
2
n_p^*
2
3
4
5
6
n_s^*